An empirical failure model to predict biofouling growth on fired bricks due to microalgae

Enrico Quagliarini[a*], Benedetta Gregorini[a], Marco D'Orazio[a]

[a] Department of Construction, Civil Engineering and Architecture (DICEA), Università Politecnica delle Marche, via Brecce Bianche, 60131 Ancona, Italy

[*] Corresponding author, Tel: +39 07212204248.
Email addresses: e.quagliarini@staff.univpm.it (E. Quagliarini), b.gregorini@pm.univpm.it (B. Gregorini), m.dorazio@univpm.it (M. D'Orazio).

Highlights

- An empirical failure model about microalgae biofouling was developed
- The model takes into account the main substrate properties influencing the growth
- It also considers the environmental temperature and relative humidity
- The model was developed and validated on fired bricks

Abstract

The purpose of this study was to provide an empirical failure model predicting the microalgae growth on fired bricks surfaces. It was developed through a numerical fitting of experimental data present in literature. It considered the substrate properties related to biofouling (i.e. porosity and roughness) of different bricks under several environmental conditions (i.e. relative humidity and temperature). Results shows that the model is able to simulate the microalgae biofouling by explicitly taking into account such influencing factor. Finally, this empirical failure model is validated on a different dataset from literature and applied to time varying temperature.

Keywords: *microalgae biofouling; fired bricks; empirical failure model; substrate properties; environmental conditions;*

1 Introduction

When porous building materials are exposed to environmental weathering, their physicals and chemicals properties interact with biological factors, leading to changes in both its compositional and structural characteristics [1–3]. The growth process and vegetative development of organisms have a direct consequence on the material due to the metabolic activity connected with the growth of living organisms [4]. The living species that commonly dwell on these materials are ranging from microscopical bacterial cells to higher plants and animals [5].

Biofouling on porous building materials is a colonization process usually started by photoautotrophic microorganisms since they only need light, water and some inorganic components to start growing [1,2]. Among these, the most recurrent groups are green microalgae and cyanobacteria, shortly named as microalgae, and they usually develop in combination, especially in the European context [6–8]. Frequent maintenance and repairing interventions are then required in order to limit aesthetical, chemical and physical degradation they may produce: both ways, either repairing or not, could ultimately cause serious losses (economical or even cultural, if cultural heritage is involved) [9,10]. In order to describe and therefore limit microalgae biofouling risk on porous building materials, in recent years researchers adopted two strategies [11]: (1) determining and thus limiting, when possible, the influencing factors of biofouling growth; (2) providing models that can simulate and then forecast the biofouling risk.

Regarding the first one, literature works mainly focused on the factors that influenced the water activity: that is defined as the water available to microorganisms to growth [6,10,12–17]. They highlighted that a combination of environmental conditions, substrate properties and intrinsic aspects of the plumbing system of buildings (i.e. leaky parts and design defects of the construction) could ensure the growth and development of microalgae. For what concerns the environmental conditions, it was demonstrated that microalgae growth occurred only at saturation conditions [13,18], that is when water can be found at liquid state. From an engineering standpoint, however, two assumption can be done: water activity can be approximated with the relative humidity *RH*, as previously demonstrated in [19] and the saturation condition safety limit can be set for $RH \geq 98\%$ [18], even though brick surface could not be wet, and water activity is only present by capillary condensation [20]. Moreover, it was proved that temperature allows microalgae to develop between about 5°C and 40°C with an optimal growth condition at about 27.5°C [18,21,22]. Out of this range, microalgae growth process is unable to start or, if already started, it stops [1,2,18,23]. In this context, porosity and roughness were outlined as the main factors concerning the substrate properties [13,24–27]. In fact, roughness promotes the adherence of microalgae to the substrate while porosity is responsible for retaining water inside the material structure. Moreover, when the materials structure and geometry, in terms of porosity and roughness, is able to afford enough water activity for microalgae to start their growth, the chemical composition of the substrate may play only a secondary role, favouring or limiting their development [28–32].

For what concern the second strategy, literature has provided a reliable model for describing microalgae growth starting from experimental measures [33]. Based on the Avrami's theory, it connects the area covered by biofouling over the time by denoting a first phase of latency (when microalgae stains are not still visible), followed by a rapid growth, and finally a stagnation phase when the covered area reaches its maximum and becomes constant over the time. Such approach was applied to several type of porous buildings materials (i.e. mortars, fired bricks and stones), under different environmental conditions and biocides surface treatments, confirming its capabilities [18,26,33–35]. However, it never explicitly and quantitatively accounts for the growth influencing factors of the substrate and environmental conditions, as failure models usually do. This way, no failure models still exist in literature for microalgae growth on porous building materials, to the authors' knowledge, while numerous failure models have been presented for other type of biofouling (e. g. mould, fungi, actinomycetes) [19,36–43].

Hence, the aim of this work is to propose a first empirical microalgae growth failure model, that is able to explicitly take into account, for the first time, the main influencing factors of substrate parameters (such as porosity and roughness) and environmental conditions (such as temperature and relative humidity), as well as their variation over the time. Fired bricks are here considered due to the availability of a large set of experimental data in literature, but the methodology can be extended to other porous building materials when enough experimental data will be available. To this aim, this work is divided into three main phases. The first phase involves the definition of: the model general requirements (Section 2.1); the variables domains (Section 2.2) and the specific model equations (Section 2.3). The fitting method is then provided (Section 2.4). Lastly, resulting equations are presented and validated and the application of the model under time varying temperature is reported (Section 3).

2 Materials and methods

2.1 General requirements

As stated above, the starting point of this work is the modified Avrami's model [34,35] showed in (1):

$$X(t) = \frac{A_C}{A_T} \cdot (1 - \exp^{-K(t-t_1)^n}) \tag{1}$$

where the covered area by microalgae growth $X(t)$ [-] is given as a function of time t [day]. The final covered area ratio is represented by the parameter A_C/A_T which expresses the percentage of the covered area at the end of the process (A_C is the maximum covered area by biofouling on a specific sample, and A_T is the total area of the same sample), K [day^{-4}] is a rate parameter determined by the least squares method using experimental measurements. Lastly, the parameter t_1 represents the latency time [day] before a chromatic variation occurs on the material surface and the coefficient n is the Avrami's coefficient which can be assumed equal to 4 [34].

The model variables are chosen according to literature findings. Porosity P [-] and roughness R [μm] are the main factors characterising the substrate [6,25,26] and, their values are easily measurable and available in literature (see Section 2.2). Temperature T [°C] and relative humidity RH [%] are instead selected as the main factors representing environmental conditions [13,14,18].

In this way:

- since literature showed that, regardless of the temperature, RH determines the actual possibility for microalgae to growth, according to which growth happens only if $RH \geq 98\%$ [18], it can be considered as an on/off factor;

- when $RH \geq 98\%$ and $5°C \leq T \leq 40°C$ growth can happen depending on *T*, *P* and *R*, otherwise it cannot [13,18];
- thus, *P*, *R* and *T* directly affect the microalgae coverage *X* through its parameters A_C/A_T, *K* and t_1 [18,26,34,35].

Inorganic compounds are here not directly considered due to their difficult measurement and their possible non-homogeneous distribution, but they are assumed as available. At the same time, an optimal day/night period is assumed to consider the influence of the light. These come from the choice of the experimental dataset (see Section 2.2). Both these assumptions can be considered as conservative standpoints.

Equation (2) shows the analytical translation of the previous requirements.

$$X(T,RH,P,R,t) = \Omega(RH)\cdot\frac{A_C}{A_T}(T,P,R)\cdot\left[1-\exp^{-K(T,P,R)\cdot\left(t-t_1(T,P,R)\right)^4}\right] \quad (2)$$

where the $\Omega(RH)$ is defined as in (3) and $5°C \leq T \leq 40°C$.

$$\Omega(RH) = \begin{cases} 0, & RH < 98\% \\ 1, & RH \geq 98\% \end{cases} \quad (3)$$

Besides, two analytical requirements over the time *t* can be stated, as reported in (4).

$$\begin{cases} X(t) = 0, \forall t < t_1(T,P,R) \\ X(t_i) \leq X(t_{i+1}), \forall t_i < t_{i+1} \end{cases} \quad (4)$$

The first one involves the latency time t_1 and it tries to overcome an analytical inaccuracy. In fact, the use of t_1 can lead to a miscalculation on the covered area: since the function is even, when the latency time is different from 0, the covered area at $t=0$ is higher than 0 with a decreasing trend between $t = 0$ and $t = t_1$. This means that the growth curve minimum is equal to 0 when $t= t_1$, too. This is not so correct from a physical description of microalgae growth, even if t_1 is usually very short if compared to the total growth time and the predicted biofouling coverage in this interval is rather poor. Thus, microalgae growth is set to be 0 until the latency time is reached. The second condition states that the model has to be a monotonically not decreasing function, that is, the reached covered area can be constant or it can increase, according to the environmental conditions. In fact, previous researches showed that, once settled, microalgae are able to retain water inside them and therefore survive i.e. dry periods [2,44].

2.2 The experimental dataset and domains determination

For the experimental dataset based on fired brick substrates, no novel experimental tests are performed, but a very large dataset coming from a previous work [18] is used. This dataset is in fact: (1) comparable to other ones of previous failure model used in literature [19,39,45,46] and (2) representative of the main influencing growing factors for microalgae, such as *P* and *R*. Moreover, it considers two of the most recurrent species of microalgae on building materials [6], namely *Chlorella mirabilis* (green microalga) and *Chroococcidiopsis fissurarum* (cyanobacterium), by accounting for them an optimal day/night period equal to 14/10 h respectively[18] and an adequate level of inorganic compound, according to ASTM D5589-09 standard method [47].

Table 1 summarizes the substrate properties (*P* and *R*) of the five fired bricks (SP_1, …, SP_5), and the seven different environmental combinations of *T* and *RH* (EC_1, …, EC_7).

Table 1. Combination of the tested substrate properties (SP) and environmental conditions (EC) [18]. Three samples were tested for each substrate property (SP).

	Substrate Properties		**Environmental Conditions** Temperature [°C] – Relative humidity [%]						
	Porosity [-]	Roughness [µm]	EC_1	EC_2	EC_3	EC_4	EC_5	EC_6	EC_7
SP_1	0.19	4.50							
SP_2	0.19	5.54							
SP_3	0.25	2.95	T=27.5 RH=75	T=27.5 RH=87	T=27.5 RH=98	T=5 RH≈100	T=10 RH≈100	T=27.5°C RH≈100	T=40 RH≈100
SP_4	0.44	6.60							
SP_5	0.44	7.60							

Materials SP_1, SP_3 and SP_5 are considered for the fitting process since they are comprehensive of the substrate domain, representing the minimum, maximum and intermediate values for both *P* and *R*. On the other hand, SP_2 and SP_4 are used in the post fitting process in order to validate its results. All the tested environmental conditions are taken into account in the fitting process. Hence, the dataset for the experimental fitting process is composed by 63 experimental microalgae growth curves, referring to 3 samples for 3 substrates under 7 different environmental conditions and by 42 curves for the validation step.

Common P and R values of fired bricks were also investigated [25–27,29,35,48–54] to see how the experimental data set (Table 1) is representative. This way, an application range for the empirical failure model can be provided. The review described 60 different brick porosity and 20 roughness values, respectively (Figure 1). It is worth noting that the (open) porosity and the roughness, usually considered in literature [25,27,29,35,48,54,55] as microalgae growing factors, are those determined according to the ASTM D4404-10 standard [56] and UNI EN ISO 4287:2009 standard[1] [57], respectively. We will refer to such references in the following.

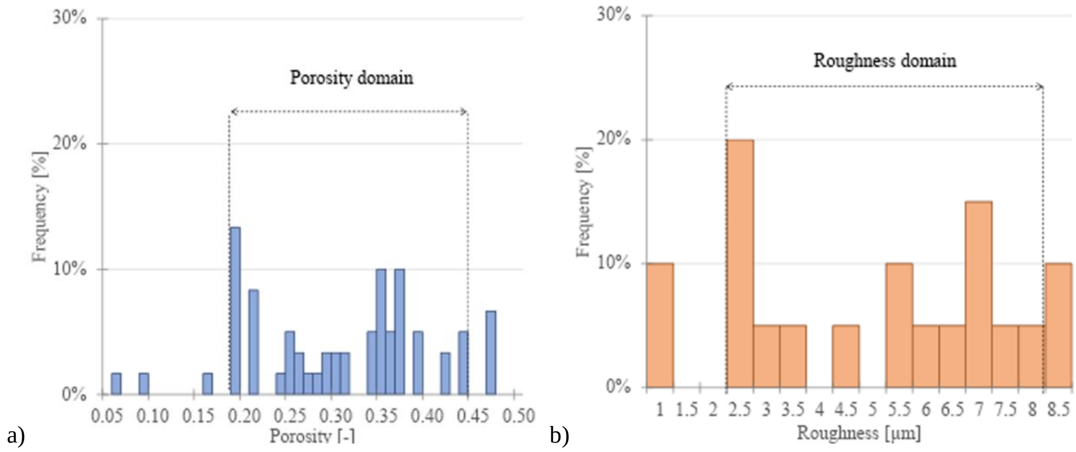

Figure 1. Comparison between porosity and roughness values from literature [25–27,29,35,48–54] and the porosity and roughness domain from the selected database [18].

By comparing the literature review results and the experimental dataset reported in Table 1, the domain for P and R is set as reported in (5).

$$\begin{cases} 0.19 \le P \le 0.44 \\ 2.50\mu m \le R \le 8.00\mu m \end{cases} \quad (5)$$

In particular, it is worth noting that the porosity domain set for the model includes 87% samples' values, while the roughness domain covers 80% of samples provided by literature.

2.3 Experimental trend and analytical model definition

Figure 2 shows the experimental trend of the parameter A_C/A_T, K and t_1 obtained from the used dataset: the parameter values refer to the specimens of the tested materials (SP_1, SP_3 and SP_5) under saturation condition (as reported in EC_4, …, EC_7), for a total of 36 experimental data for each parameter. In the between of domain, T

[1] Roughness values were determined according to R_a calculation.

predominantly influences A_C/A_T and K, determining an increasing trend from 5°C to about 27.5°C and a decreasing one from about 27.5°C to 40°C. These trends hold for each P and R. Lastly, in Figure 2 (c) the latency time t_1 shows a constant trend not depending on temperature, conversely, it is influenced by P and R.

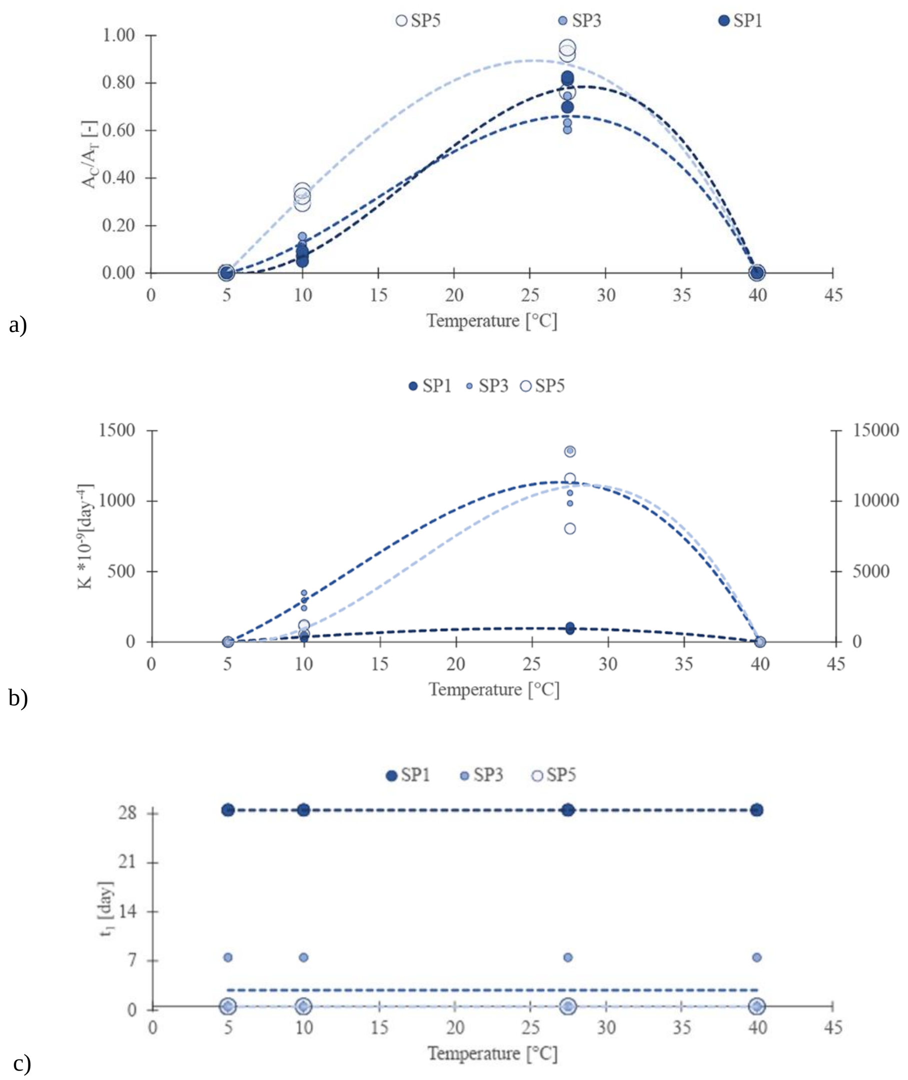

Figure 2. Experimental trend of bricks parameters: (a) A_C/A_T parameter; (b) K parameter; (c) t_1 parameter. The graphs are reported according to the temperature domain. The blue scale (dark-light) indicates the increasing porosity; the increasing dimension of the spot indicates the increasing roughness value. In (b) two y-axis were used since the K parameters are significantly different: SP_1 and SP_3 refer to the left y-axis, SP_5 refers to the right y-axis.

In this way, aiming at determining the simplest possible model, having only 4 different temperature values, a 3rd degree polynomial is set in order to describe A_C/A_T and K as functions of T, having its coefficients depending on P and R. For the t_1 parameter, a constant coefficient depending only on P and R is set. The above observations are reported in (6):

$$\begin{cases} \dfrac{A_C}{A_T}(T,P,R) = c_{0,A}(P,R) + c_{1,A}(P,R)\cdot T + c_{2,A}(P,R)\cdot T^2 + c_{3,A}(P,R)\cdot T^3 \\ K(T,P,R) = c_{0,K}(P,R) + c_{1,K}(P,R)\cdot T + c_{2,K}(P,R)\cdot T^2 + c_{3,K}(P,R)\cdot T^3 \\ t_1(P,R) = c_{0,t}(P,R) \end{cases} \tag{6}$$

where the coefficients reported in (6) result from the fitting process (see Section 2.4).

Finally, the codomains of each involved parameter are reported in equation (7):

$$\begin{cases} 0 \le \dfrac{A_C}{A_T}(T,P,R) \le 1 \\ K(T,P,R) \ge 0 \qquad , \ \forall T \in [5;40], \forall P \in [0.19;0.44], \forall R \in [2.50;8.00] \\ t_1(P,R) \ge 0 \end{cases} \tag{7}$$

2.4 The fitting process

From condition (6), a linear system of the temperature coefficient can be set as in (8).

$$\begin{cases} c_{n,A} = \alpha_{n,1,A}F_{1,A}(P,R) + \alpha_{n,2,A}F_{2,A}(P,R) + \alpha_{n,3,A}F_{3,A}(P,R) \\ c_{n,K} = \alpha_{n,1,K}F_{1,K}(P,R) + \alpha_{n,2,K}F_{2,K}(P,R) + \alpha_{n,3,K}F_{3,K}(P,R), \quad n = 0,...,3 \\ c_{0,t} = \alpha_{0,1,t}F_{1,t}(P,R) + \alpha_{n,2,t}F_{2,t}(P,R) + \alpha_{n,3,t}F_{3,t}(P,R) \end{cases} \tag{8}$$

The $F_1,\ldots, F_3$ considered the effect of *P* and *R* values and they are defined in (9)

$$\begin{cases} F_1(P,R) \in \left\{P^{j_1}, R^{k_1}, 0\right\} \\ F_2(P,R) \in \left\{P^{j_2}, R^{k_2}, 0\right\}, \quad j_1,..., j_3, k_1,..., k_3 \in \mathbb{Z} \\ F_3(P,R) \in \left\{P^{j_3}, R^{k_3}, 0\right\} \end{cases} \tag{9}$$

This means that the combination of $F_1,\ldots, F_3$ can consider only *P* element, conversely only *R* elements, it may be resumed in a constant value (e.g. for *j* and *k* exponent resulting equal to 0) or even it can result equal to 0. This is due because the trends for both *P* and *R* were not clearly obtainable from the experimental evidences [18], and therefore determined in advanced as for temperature.

Hence, once set conditions (8)-(9), the fitting process is iteratively run by determining the α values and the right combination of $F_1,\ldots, F_3$ for the three parameters, following what is reported in (10) where $F_1,\ldots, F_3$ have the same degree for each surface properties SP.

$$\begin{cases} \begin{vmatrix} \alpha_{0,1} & \alpha_{0,2} & \alpha_{0,3} \\ \alpha_{1,1} & \alpha_{1,2} & \alpha_{1,3} \\ \alpha_{2,1} & \alpha_{2,2} & \alpha_{2,3} \\ \alpha_{3,1} & \alpha_{3,2} & \alpha_{3,3} \end{vmatrix} \begin{vmatrix} F_1(P,R) \\ F_2(P,R) \\ F_3(P,R) \end{vmatrix}_{SP1} = \begin{vmatrix} c_0 \\ c_1 \\ c_2 \\ c_3 \end{vmatrix}_{SP1} \\ \begin{vmatrix} \alpha_{0,1} & \alpha_{0,2} & \alpha_{0,3} \\ \alpha_{1,1} & \alpha_{1,2} & \alpha_{1,3} \\ \alpha_{2,1} & \alpha_{2,2} & \alpha_{2,3} \\ \alpha_{3,1} & \alpha_{3,2} & \alpha_{3,3} \end{vmatrix} \begin{vmatrix} F_1(P,R) \\ F_2(P,R) \\ F_3(P,R) \end{vmatrix}_{SP3} = \begin{vmatrix} c_0 \\ c_1 \\ c_2 \\ c_3 \end{vmatrix}_{SP3} \\ \begin{vmatrix} \alpha_{0,1} & \alpha_{0,2} & \alpha_{0,3} \\ \alpha_{1,1} & \alpha_{1,2} & \alpha_{1,3} \\ \alpha_{2,1} & \alpha_{2,2} & \alpha_{2,3} \\ \alpha_{3,1} & \alpha_{3,2} & \alpha_{3,3} \end{vmatrix} \begin{vmatrix} F_1(P,R) \\ F_2(P,R) \\ F_3(P,R) \end{vmatrix}_{SP5} = \begin{vmatrix} c_0 \\ c_1 \\ c_2 \\ c_3 \end{vmatrix}_{SP5} \end{cases} \tag{10}$$

The process stops when the following two requirements are achieved. The first requirement verifies the analytical correctness of the model by determining the adjusted coefficient of determination R^2_{adj} since a multiple variable regression is considered. The calculation of R^2_{adj} is shown in equation (11) and all the R^2_{adj} have to be higher than 0.85. Such limit was previously adopted in other models to consider the accuracy of the fitting good [58–60].

$$R^2_{adj} = 1 - \frac{RSS}{TSS} \cdot \frac{n-1}{n-p-1} \geq 0.85 \tag{11}$$

The *RSS* is the residual sum of squares between the experimental and the fitted data, *TSS* is the total sum of squares of the differences between the experimental data and its mean, *n* is the number of observation and *p* is the total number of explanatory variables in the model [61].

Subsequently, the second requirement involves the experimental correctness of the model. It is satisfied when conditions reported in (12) are fulfilled.

$$\begin{cases} \min\left[\dfrac{A_C}{A_T}_{\text{exp}}\right] \le \dfrac{A_C}{A_T}(T,P,R) \le \max\left[\dfrac{A_C}{A_T}_{\text{exp}}\right] \\ \min\left[K_{\text{exp}}\right] \le K(T,P,R) \le \max\left[K_{\text{exp}}\right] \\ \min\left[t_{1,\text{exp}}\right] \le t_1(P,R) \le \max\left[t_{1,\text{exp}}\right] \end{cases} \quad (12)$$

After having defined all the parameters with their coefficients, the failure model is tested on SP_2 and SP_4 so as to have a first validation, following the same criteria: R^2_{adj} still has to be higher than 0.85, as analytical requirement and the experimental correctness must be verified by conditions reported in (12).

3 Results

3.1 The failure model for bricks

Condition (13) summarise the resulting α values and the combinations of F_1,…, F_3 of each parameter, by also resuming condition (6) for the temperature equations.

$$
\begin{cases}
\frac{A_C}{A_T}(T,P,R)=\begin{vmatrix}
-3.419[-] & 9.2\cdot10^{-2}\left[\frac{1}{\mu m}\right] & -5.7\cdot10^{-3}\left[\frac{1}{\mu m^2}\right]\\
8.798\cdot10^{-1}\left[\frac{1}{°C}\right] & -3.1032\cdot10^{-2}\left[\frac{1}{\mu m\cdot°C}\right] & 2.16\cdot10^{-3}\left[\frac{1}{\mu m^2\cdot°C}\right]\\
-3.98\cdot10^{-2}\left[\frac{1}{°C^2}\right] & 2.8023\cdot10^{-3}\left[\frac{1}{\mu m\cdot°C^2}\right] & -2.184\cdot10^{-4}\left[\frac{1}{\mu m^2\cdot°C^2}\right]\\
5\cdot10^{-4}\left[\frac{1}{°C^3}\right] & -5.21\cdot10^{-5}\left[\frac{1}{\mu m\cdot°C^3}\right] & 4.198\cdot10^{-6}\left[\frac{1}{\mu m^2\cdot°C^3}\right]
\end{vmatrix}\begin{vmatrix}P^2\\R\\R^2\end{vmatrix}\cdot\begin{vmatrix}T^0\\T^1\\T^2\\T^3\end{vmatrix}\\
K(T,P,R)=\begin{vmatrix}
-1.018137\cdot10^{-6}\left[day^{-4}\right] & 2.638435\cdot10^{-5}\left[day^{-4}\right] & -1.109344\cdot10^{-3}\left[\mu m^8\cdot day^{-4}\right]\\
3.832828\cdot10^{-7}\left[\frac{day^{-4}}{°C}\right] & -1.056712\cdot10^{-5}\left[\frac{day^{-4}}{°C}\right] & 2.729806\cdot10^{-4}\left[\frac{\mu m^8\cdot day^{-4}}{°C}\right]\\
-3.978387\cdot10^{-8}\left[\frac{day^{-4}}{°C^2}\right] & 1.173803\cdot10^{-6}\left[\frac{day^{-4}}{°C^2}\right] & -1.081282\cdot10^{-5}\left[\frac{\mu m^8\cdot day^{-4}}{°C^2}\right]\\
7.709831\cdot10^{-10}\left[\frac{day^{-4}}{°C^3}\right] & -2.315303\cdot10^{-8}\left[\frac{day^{-4}}{°C^3}\right] & 1.169671\cdot10^{-7}\left[\frac{\mu m^8\cdot day^{-4}}{°C^3}\right]
\end{vmatrix}\begin{vmatrix}P\\P^3\\R^{-8}\end{vmatrix}\cdot\begin{vmatrix}T^0\\T^1\\T^2\\T^3\end{vmatrix}\\
t_1(P,R)=\begin{vmatrix}4.73\cdot10^{-5}[day] & -2.88\cdot10^{-4}\left[\frac{day}{\mu m}\right] & -2.66\cdot10^{-4}\left[\frac{day}{\mu m^2}\right]\end{vmatrix}\begin{vmatrix}P^{-8}\\R\\R^2\end{vmatrix}
\end{cases}
\qquad (13)
$$

Figure 3 shows that all the R^2_{adj} are higher than 0.85 for A_C/A_T, K and t_1.

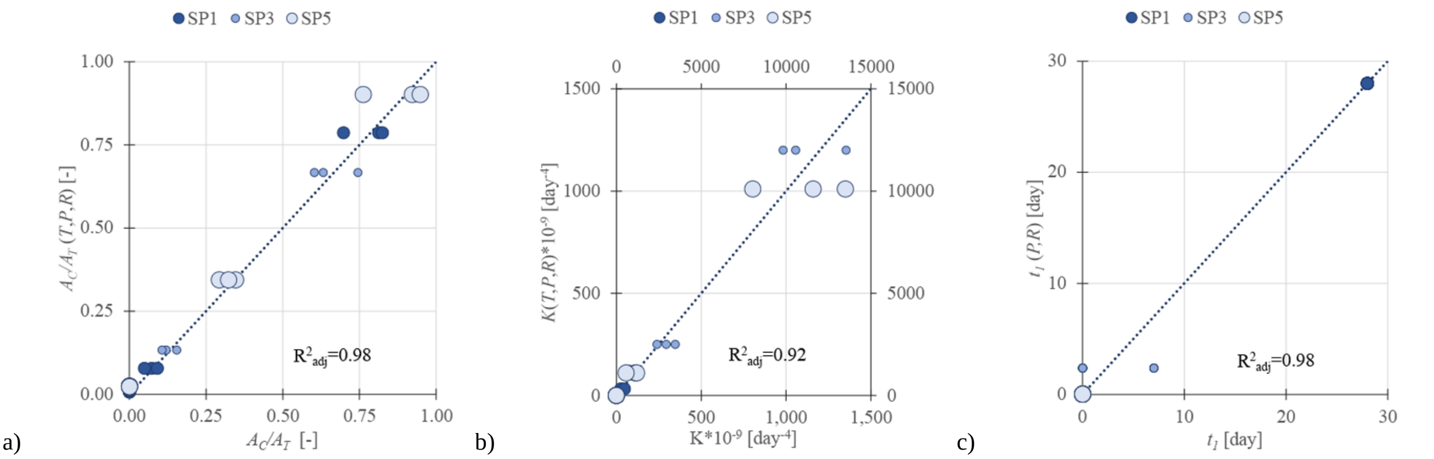

Figure 3. Coefficient of determination R^2 of the parameter. (a) A_C/A_T parameters; (b) K parameter; (c) t_1 parameter. The blue scale (dark-light) indicates the increasing porosity the increasing dimension of the spot indicates the increasing roughness value. In (b) two y-axis were used since the K parameters are significantly different: SP_1 and SP_3 refer to the left y-axis, SP_5 refers to the right y-axis.

Lasty, both the experimental values and the fitted curves are reported in Figure 4. These last ones falls within the experimental values, verifing the condition proposed in (12).

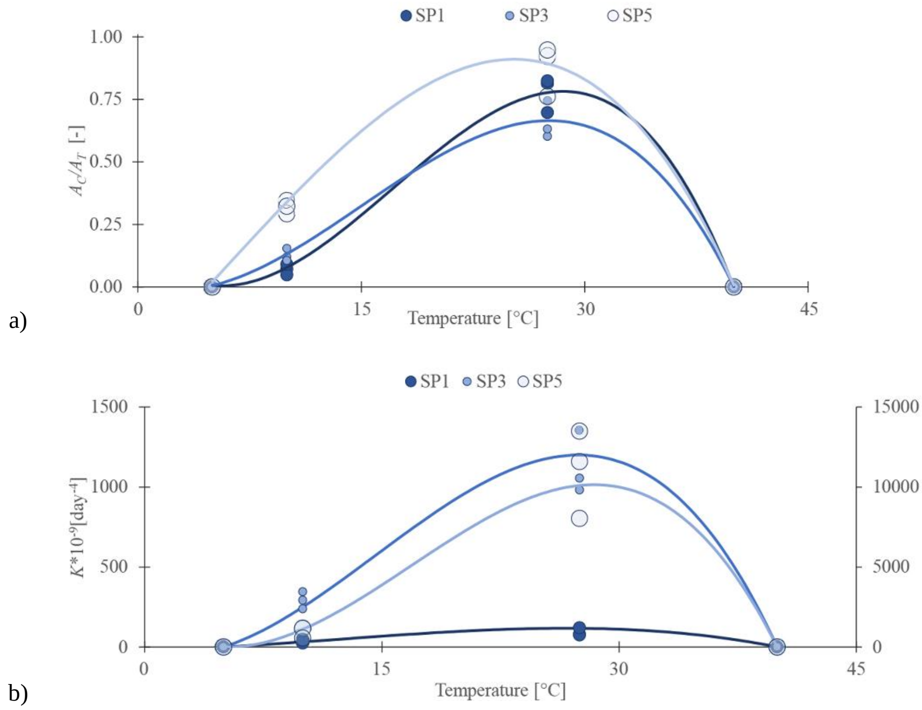

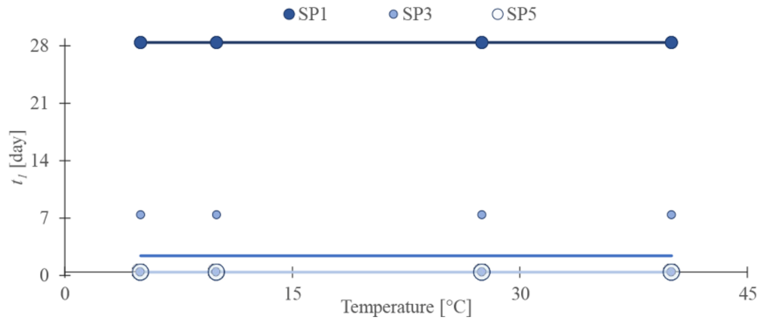

c)

Figure 4. Comparison between the the experimental values and the fitted curves for the sufaces properties SP_1 SP_3 and SP_5: (a) A_C/A_T (b) K and (c) t_1. The blue scale (dark-light) indicates the increasing porosity; the increasing dimension of the spot indicates the increasing roughness value. In (b) two y-axis were used since the K parameters are significantly different: SP_1 SP_3 refer to the left y-axis, SP_5 refers to the right y-axis.

3.2 Failure model validation

The failure model is then applied on the second dataset. As shown in Figure 5, the three R^2_{adj} were always higher than 0.85.

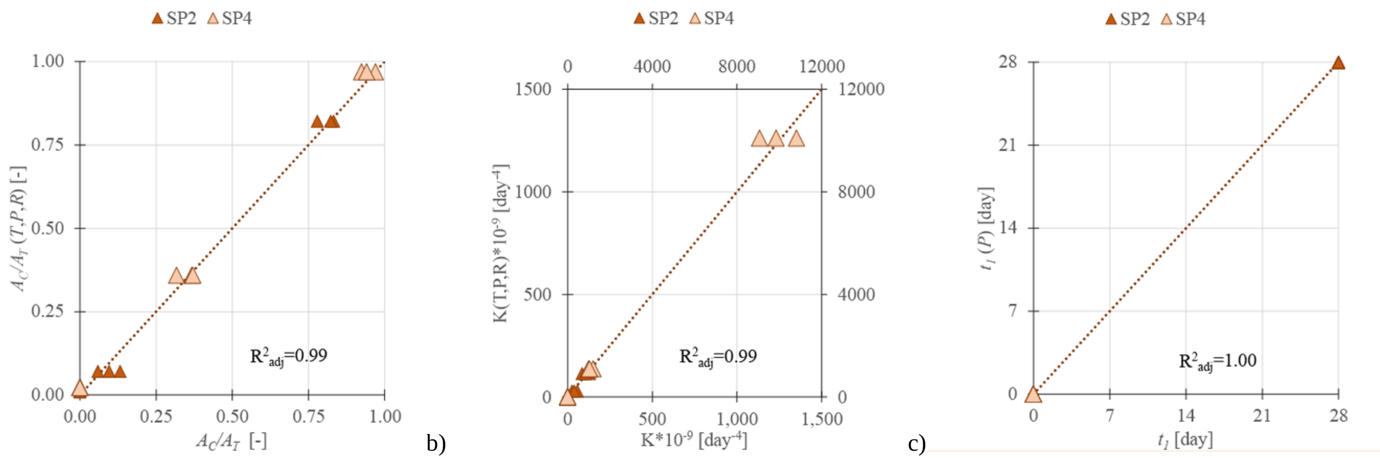

a) b) c)

Figure 5. Coefficient of determination R^2 of the parameters. (a) A_C/A_T parameters; (b) K parameter; (c) t_1 parameter. The red scale (dark-light) indicates the increasing porosity; the increasing dimension of the spot indicates the increasing roughness value. In (b) two y-axis were used since the K parameters are significantly different: SP_2 refer to the left y-axis, SP_4 refers to the right y-axis.

Figure 6, instead, shows that the curves determined by the failure model fell within the range of their respective experimental data.

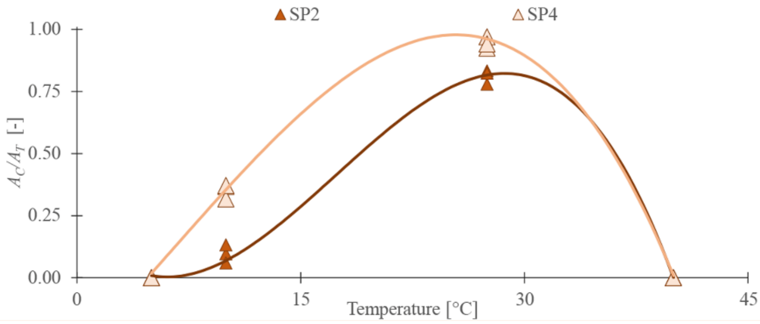

a)

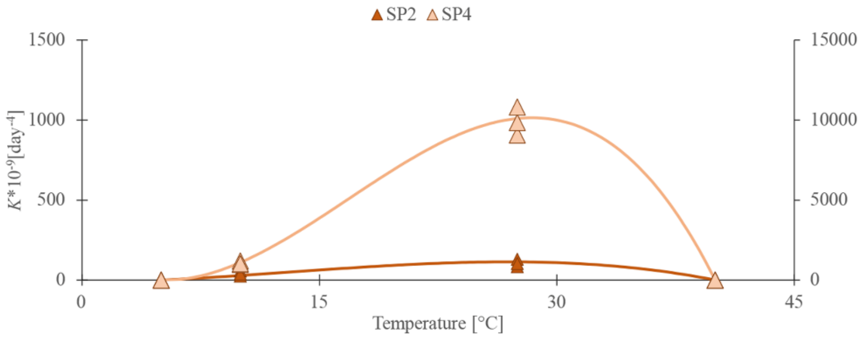

b)

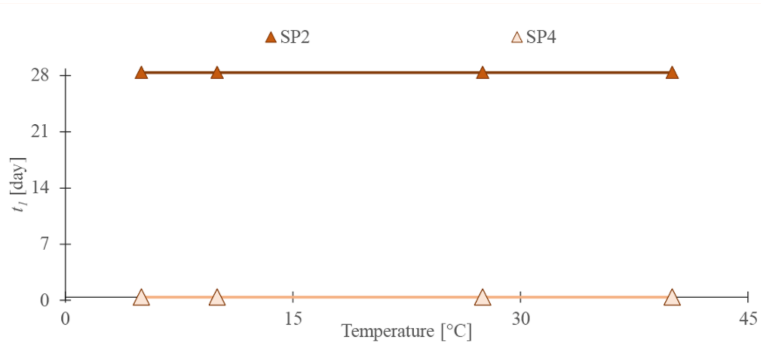

c)

Figure 6. Comparison between the the experimental values and the fitted curves for the sufaces properties SP_2 and SP_4: (a) A_C/A_T (b) K and (c) t_1. The dotted red lines indicate the minimum and maximum curve for P and R values. The red scale (dark-light) indicates the increasing porosity; the dimension of the spot (6-7) indicates the roughness value. In (b) two y-axis were used since the K parameters are significantly different: SP_2 refers to the left y-axis, SP_4 refers to the right y-axis.

As a last qualitative validation step, according to other previous model validation [39,46], the curves describing microalgae growth $X(t, T, RH, P, R)$ are determined for the validation substrates SP_2 and SP_4 under the tested environmental condition EC_5 and EC_6 (Table 1) and overlapped to the experimental data obtained in [18]. All the curves well fit the experimental values (Figure 7).

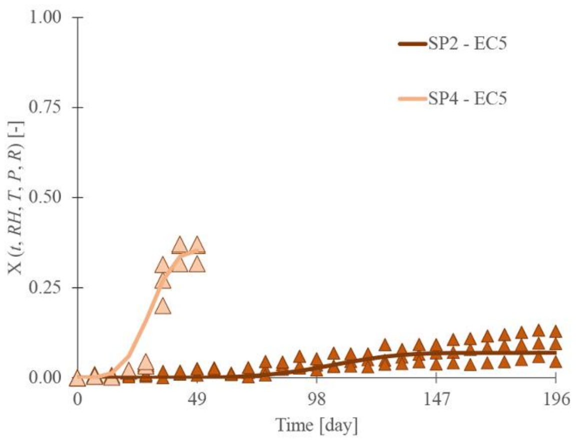

a)

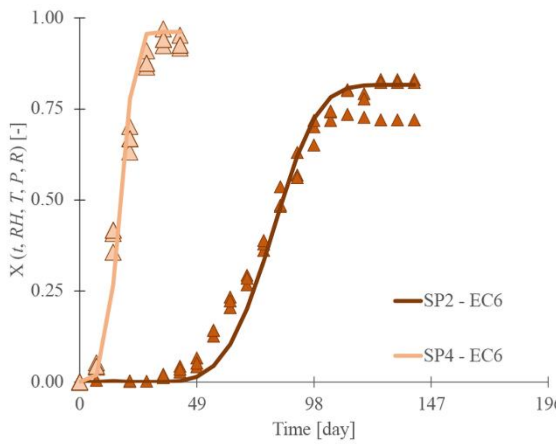

b)

Figure 7. Comparison of the covered area X(t, T, RH, P, R) obtained with the failure model and experimental data for SP_2, and SP_4 [18]:a) when exposed to EC_5;b) when exposed to EC_6. Lines indicate the failure model curves; points indicate the experimental data.

3.3 Failure model application over time-variable environmental conditions

Lastly, this paragraph shows the model application for a representative brick substrate exposed to time-variable environmental conditions (Table 2).

Table 2. Specification for the model application.

Material		Condition (C)		
Porosity [-]	Roughness [µm]	n°	Temperature [°C]	Exposure Time [day]
0.19	2.75µm	1	14	50
		2	7.5	50
		3	20	50
		4	27.5	50

The brick properties are chosen in order to describe the most recurrent ones according to Figure 1. The assumed four conditions do not simulate a real dataset, but they allow improving the readability of the combination process. In particular, the gradient between the four temperatures values allows having four distinctive branches that significantly differ from each other and the exposure time of 50 days led the growth process for each condition be clearly recognizable. Lastly, time and the time dependent variable (*T* and *RH*) are daily discretized and kept constant during the day for sake of simplicity.

The combination of the branches over the time is made by following these 2 assumptions: (1) *P* and *R* are given and they both cannot change; (2) the coverage cannot go back and decrease, as already stated in equation (4). Hence, each involved *n*-branch of each *T*-dependent curve is joined to another *n+1*-curve by simply determining the time shift $t_{s,n}$ following simple steps from equation as reported in equation (14):

$$t_{s,n} = +\sqrt[4]{-\left(\frac{1}{K(T_{n+1})}\right)\cdot \ln\left(1-\frac{X_n}{\frac{A_C}{A_T}(T_{n+1})}\right)} - t + t_1 \qquad (14)$$

The logarithmic calculation is possible only if the reached covered area X_n is lower than the A_C/A_T (T_{n+1}), otherwise the covered area is kept constant over the time.

Figure 8. shows the graphical combination of such branches and the resulting curve under time variable environmental conditions. In Figure 8. (a), the *T*-curves are determined and each branch for the corresponding exposure time is selected. Since the covered area of C_1 ($X_{n=1}$) is higher than the A_C/A_T ($T_{n=2}$), the latency time is not determined, and hence, for all the C_2 exposure time the covered area is maintained constant. Figure 8. (b) shows the resulting combination of the branches for C_1, C_3 and C_4 and the constant growth curve for T=7.5°C.

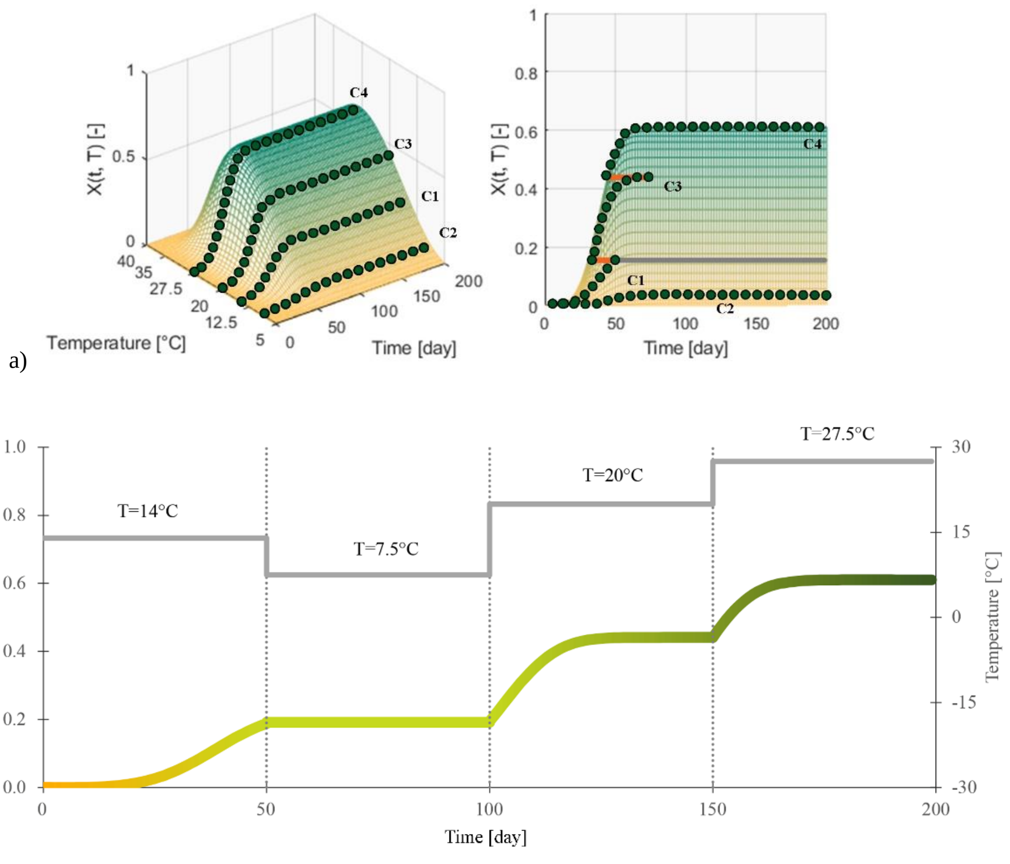

Figure 8. Application of the model to time changing environmental conditions: a) combination methods; b) resulting curve for temperature variation over time. In (a) the covered area is following the colour scale green-yellow resembling microalgae biofouling effect; dots represent the selected curve; lines orange indicate the combination effect of the time shift; line grey indicates that it was not possible to determine the time shift; in (b) the colour scale yellow green is maintained for the total microalgae curve.

4 Conclusion

Failure models for biofouling on building materials are becoming a more and more unavoidable need: by making quantitative predictions, they can assist professionals and researchers in developing guidelines for interventions leading to a decrease in maintenance costs. Literature have already provided such models for mould and fungi growth, but it is still limited for microalgae growth. This work tries to fill this gap by presenting a novel empirical failure model for fired bricks by taking into account the main substrate and environmental parameters influencing such growth, which are porosity and roughness, as well as temperature and relative humidity. It starts from the modified Avrami's model, by determining its three main parameters from experimental results, by also improving it about some miscalculations in the range of the latency time. From the obtained results, it is evident that such model is analytically intuitive and easy to implement. From an engineering standpoint, the novel empirical model seems to be generally applicable since the tested domain of porosity and roughness covers more than 80% of the fired bricks reported in literature. Finally, the application of such model considering time variable environmental conditions is proposed too.

Future works should consider more brick type and different environmental conditions as soon as experimental data will be available. Once confirmed its correctness for bricks, the model application could be extended to other porous building materials (such as i.e. stones, plasters and mortars) prone to microalgae growth. Moreover, thanks to its ability of considering time varying environmental conditions the model could be implemented on heat and moisture simulation software, as it is already happening for other biofouling models. This will lead to the application of the failure model to a real weather dataset, even considering the water content of the substrate instead of solely relative humidity.

Acknowledgements

This research did not receive any specific grant from funding agencies in the public, commercial, or not-for-profit sectors.

Nomenclature

Experimental parameters by literature researches (based on modified Avrami's Theory)	
X	covered area by microalgae biofouling [-]
A_C/A_T	parameter of final covered area ratio [-]
K	parameter of growth rate [day^{-4}]
t_1	parameter of latency time [day]
Fitted parameters (failure model)	
$X(t, T, RH, P, R)$	covered area by microalgae biofouling [-]
$A_C/A_T\ (T, P, R)$	parameter of final covered area ratio [-]
$K\ (T, P, R)$	parameter of growth rate [day^{-4}]
$t_1\ (P, R)$	parameter of latency time [day]
$\Omega(RH)$	on off parameter for relative humidity [-]
Variables	
t	time [day]
T	temperature [°C]
RH	relative humidity [%]
P	total porosity [%]
R	roughness [µm]
Coefficients	
c	temperature equation coefficient
α	coefficient for material properties
F	element describing the effect of P or R
Subscript and Superscript	
$_n$	number of temperature coefficients, from 0 to 3
$_{1,2,3}$	number of material coefficient for both α and F values

j	number of coefficient/exponents for porosity
k	number of coefficient/exponents for roughness

References

[1] P. Tiano, Biodegradation of Cultural Heritage: Decay Mechanisms and Control Methods, 9th ARIADNE Work. "Historic Mater. Their Diagnostic." (2002) 1–37. doi:10.1.1.129.3386.

[2] G. Caneva, M.P. Nugari, O. Salvadori, Biology in the Conservation of Works of Art, ICCROM, 1991.

[3] C. Ferrari, G. Santunione, A. Libbra, A. Muscio, E. Sgarbi, C. Siligardi, G.S. Barozzi, Review on the influence of biological deterioration on the surface properties of building materials: Organisms, materials, and methods, Int. J. Des. Nat. Ecodynamics. 10 (2015) 21–39. doi:10.2495/DNE-V10-N1-21-39.

[4] O. Guillitte, Bioreceptivity: a new concept for building ecology studies, Sci. Total Environ. 167 (1995) 215–220. doi:10.1016/0048-9697(95)04582-L.

[5] T. Warscheid, J. Braams, Biodeterioration of stone: a review, Int. Biodeterior. Biodegradation. 46 (2000) 343–368. doi:10.1016/S0964-8305(00)00109-8.

[6] H. Barberousse, B. Ruot, C. Yéprémian, G. Boulon, An assessment of façade coatings against colonisation by aerial algae and cyanobacteria, Build. Environ. 42 (2007) 2555–2561. doi:10.1016/j.buildenv.2006.07.031.

[7] M.L. Coutinho, A.Z. Miller, M.F. Macedo, Biological colonization and biodeterioration of architectural ceramic materials: An overview, J. Cult. Herit. 16 (2015) 759–777. doi:10.1016/j.culher.2015.01.006.

[8] C.C. Gaylarde, P.M. Gaylarde, A comparative study of the major microbial biomass of biofilms on exteriors of buildings in Europe and Latin America, Int. Biodeterior. Biodegrad. 55 (2005) 131–139. doi:10.1016/j.ibiod.2004.10.001.

[9] C. Gaylarde, M. Ribas Silva, T. Warscheid, Microbial impact on building materials: an overview, Mater. Struct. 36 (2003) 342–352. doi:10.1007/BF02480875.

[10] I. Flores-Colen, J. de Brito, V.P. de Freitas, Stains in facades' rendering - Diagnosis and maintenance techniques' classification, Constr. Build. Mater. 22 (2008) 211–221. doi:10.1016/j.conbuildmat.2006.08.023.

[11] T. Verdier, M. Coutand, A. Bertron, C. Roques, A review of indoor microbial growth across building

materials and sampling and analysis methods, Build. Environ. 80 (2014) 136–149. doi:10.1016/J.BUILDENV.2014.05.030.

[12] P. Johansson, Determination of the Critical Moisture Level for Mould Growth on Building Materials, 2014.

[13] D. Giovannacci, C. Leclaire, M. Horgnies, M. Ellmer, J.D. Mertz, G. Orial, J. Chen, F. Bousta, Algal colonization kinetics on roofing and façade tiles: Influence of physical parameters, Constr. Build. Mater. 48 (2013) 670–676. doi:10.1016/j.conbuildmat.2013.07.034.

[14] H. Barberousse, R.J. Lombardo, G. Tell, A. Couté, Factors involved in the colonisation of building façades by algae and cyanobacteria in France, Biofouling. 22 (2006) 69–77. doi:10.1080/08927010600564712.

[15] O. Guillitte, R. Dreesen, Laboratory chamber studies and petrographical analysis as bioreceptivity assessment tools of building materials, Sci. Total Environ. 167 (1995) 365–374. doi:10.1016/0048-9697(95)04596-S.

[16] F. Gladis, R. Schumann, Influence of material properties and photocatalysis on phototrophic growth in multi-year roof weathering, Int. Biodeterior. Biodegradation. 65 (2011) 36–44. doi:10.1016/J.IBIOD.2010.05.014.

[17] C.A. Crispim, P.M. Gaylarde, C.C. Gaylarde, Algal and cyanobacterial biofilms on calcareous historic buildings, Curr. Microbiol. 46 (2003) 79–82. doi:10.1007/s00284-002-3815-5.

[18] E. Quagliarini, A. Gianangeli, M. D’Orazio, B. Gregorini, A. Osimani, L. Aquilanti, F. Clementi, Effect of temperature and relative humidity on algae biofouling on different fired brick surfaces, Constr. Build. Mater. 199 (2019) 396–405. doi:10.1016/J.CONBUILDMAT.2018.12.023.

[19] A. Hukka, H. Viitanen, A mathematical model of mould growth on wooden material, Wood Sci. Technol. 33 (1999) 475–485. doi:10.1007/s002260050131.

[20] A. Stazi, M. D’Orazio, E. Quagliarini, In-life prediction of hygrometric behaviour of buildings materials: an application of fractal geometry to the determination of adsorption and suction properties, Build. Environ. 37 (2002) 733–739. doi:10.1016/S0360-1323(01)00064-6.

[21] J.A. Raven, R.J. Geider, Temperature and algal growth, New Phytol. 110 (1988) 441–461.

doi:10.1111/j.1469-8137.1988.tb00282.x.

[22] K. Lengsfeld, M. Krus, Microorganism on façades – reasons, consequences and measures, (2001) 0–7.

[23] A. Konopka, T.D. Brock, Effect of temperature on blue-green algae (Cyanobacteria) in Lake Mendota, Appl. Environ. Microbiol. 36 (1978) 572–576. doi:10.1520/C1421-10.2.

[24] T.H. Tran, A. Govin, R. Guyonnet, P. Grosseau, C. Lors, E. Garcia-Diaz, D. Damidot, O. Devès, B. Ruot, Influence of the intrinsic characteristics of mortars on biofouling by Klebsormidium flaccidum, Int. Biodeterior. Biodegradation. 70 (2012) 31–39. doi:10.1016/J.IBIOD.2011.10.017.

[25] M. D'Orazio, G. Cursio, L. Graziani, L. Aquilanti, A. Osimani, F. Clementi, C. Yéprémian, V. Lariccia, S. Amoroso, Effects of water absorption and surface roughness on the bioreceptivity of ETICS compared to clay bricks, Build. Environ. 77 (2014) 20–28. doi:10.1016/j.buildenv.2014.03.018.

[26] L. Graziani, E. Quagliarini, M. D'Orazio, The role of roughness and porosity on the self-cleaning and anti-biofouling efficiency of TiO2-Cu and TiO2-Ag nanocoatings applied on fired bricks, Constr. Build. Mater. 129 (2016) 116–124. doi:10.1016/j.conbuildmat.2016.10.111.

[27] L. Graziani, E. Quagliarini, A. Osimani, L. Aquilanti, F. Clementi, M. D'Orazio, The influence of clay brick substratum on the inhibitory efficiency of TiO2 nanocoating against biofouling, Build. Environ. 82 (2014) 128–134. doi:10.1016/j.buildenv.2014.08.013.

[28] A.Z. Miller, P. Sanmartín, L. Pereira-Pardo, A. Dionísio, C. Saiz-Jimenez, M.F. Macedo, B. Prieto, Bioreceptivity of building stones: A review, Sci. Total Environ. 426 (2012) 1–12. doi:10.1016/j.scitotenv.2012.03.026.

[29] P. Tiano, P. Accolla, L. Tomaselli, Phototrophic biodeteriogens on lithoid surfaces: An ecological study, Microb. Ecol. 29 (1995) 299–309. doi:10.1007/BF00164892.

[30] A.Z. Miller, A. Dionísio, L. Laiz, M.F. Macedo, C. Saiz-Jimenez, The influence of inherent properties of building limestones on their bioreceptivity to phototrophic microorganisms, 2009. https://link.springer.com/content/pdf/10.1007%2FBF03179212.pdf (accessed December 3, 2018).

[31] A.Z. Miller, M.A. Rogerio-Candelera, L. Laiz, J. Wierzchos, C. Ascaso, M.A. Sequeira Braga, M.

Hernández-Mariné, A. Maurício, A. Dionísio, M.F. Macedo, C. Saiz-Jimenez, Laboratory-induced endolithic growth in calcarenites: Biodeteriorating potential assessment, Microb. Ecol. 60 (2010) 55–68. doi:10.1007/s00248-010-9666-x.

[32] A.Z. Miller, N. Leal, L. Laiz, M.A. Rogerio-Candelera, R.J.C. Silva, A. Dionísio, M.F. Macedo, C. Saiz-Jimenez, Primary bioreceptivity of limestones used in southern European monuments, Geol. Soc. Spec. Publ. 331 (2010) 79–92. doi:10.1144/SP331.6.

[33] T.H. Tran, A. Govin, R. Guyonnet, P. Grosseau, C. Lors, D. Damidot, O. Devès, B. Ruot, Avrami's law based kinetic modeling of colonization of mortar surface by alga Klebsormidium flaccidum, Int. Biodeterior. Biodegrad. 79 (2013) 73–80. doi:10.1016/j.ibiod.2012.12.012.

[34] L. Graziani, E. Quagliarini, On the Modelling of Algal Biofouling Growth on Nano-TiO2 Coated and Uncoated Limestones and Sandstones, Coatings. 8 (2018) 54. doi:10.3390/coatings8020054.

[35] L. Graziani, E. Quagliarini, M. D'Orazio, TiO2-treated different fired brick surfaces for biofouling prevention: Experimental and modelling results, Ceram. Int. 42 (2016) 4002–4010. doi:10.1016/j.ceramint.2015.11.069.

[36] International Energy Agency, Guidelines and Practice, Annex XIV Condens. Energy. (1990). http://www.ecbcs.org/docs/annex_14_guidelines_and_practice.pdf.

[37] N.J. Rowan, C.M. Johnstone, R.C. McLean, J.G. Anderson, J.A. Clarke, Prediction of toxigenic fungal growth in buildings by using a novel modelling system, Appl. Environ. Microbiol. 65 (1999) 4814–4821.

[38] J.A. Clarke, C.M. Johnstone, N.J. Kelly, R.C. McLean, J.A. Anderson, N.J. Rowan, J.E. Smith, A technique for the prediction of the conditions leading to mould growth in buildings, Build. Environ. 34 (1999) 515–521. doi:10.1016/S0360-1323(98)00023-7.

[39] T. Ojanen, H. Viitanen, R. Peuhkuri, K. Lähdesmäki, J. Vinha, K. Salminen, Mold Growth Modeling of Building Structures Using Sensitivity Classes of Materials, Therm. Perform. Exter. Envel. Build. XI. (2010) 1–10. doi:10.1081/E-EEE2-120046011.

[40] K. Sedlbauer, Prediction of mould fungus formation on the surface of and inside building components,

2001. http://www.ibp.fraunhofer.de/content/dam/ibp/en/documents/ks_dissertation_etcm1021-30729.pdf.

[41] M. Krus, R. Kilian, K. Sedlbauer, Mould growth prediction by computational simulation on historic buildings, Museum Microclim. (2007) 185–189.

[42] 6-3-05/D WTA Merkblatt, Rechnerische Prognose des Schimmelpilzwachstumsrisikos, Fraunhofer IRB Versl. (2006).

[43] G. Arya, J. Singh, A mathematical model to predict Actinomycetes growth in building material, Int. J. Interdiscip. Res. Innov. 4 (2016) 88–96.

[44] S.P. Shukla, J. Kvíderová, J. Tříska, J. Elster, Chlorella mirabilis as a potential species for biomass production in low-temperature environment, Front. Microbiol. 4 (2013) 1–12. doi:10.3389/fmicb.2013.00097.

[45] S. Thelandersson, T. Isaksson, Mould resistance design (MRD) model for evaluation of risk for microbial growth under varying climate conditions, Build. Environ. 65 (2013) 18–25. doi:10.1016/J.BUILDENV.2013.03.016.

[46] J. Berger, H. Le Meur, D. Dutykh, D.M. Nguyen, A.C. Grillet, Analysis and improvement of the VTT mold growth model: Application to bamboo fiberboard, Build. Environ. 138 (2018) 262–274. doi:10.1016/j.buildenv.2018.03.031.

[47] ASTM D5589-09. Standard test method for determining the resistance of paint films and related coatings to algal defacement. American Society for Testing and Materials, (2009).

[48] L. Graziani, E. Quagliarini, A. Osimani, L. Aquilanti, F. Clementi, C. Yéprémian, V. Lariccia, S. Amoroso, M. D’Orazio, Evaluation of inhibitory effect of TiO2 nanocoatings against microalgal growth on clay brick façades under weak UV exposure conditions, Build. Environ. 64 (2013) 38–45. doi:10.1016/j.buildenv.2013.03.003.

[49] A. Viani, G. Cultrone, K. Sotiriadis, R. Ševčík, P. Šašek, The use of mineralogical indicators for the assessment of firing temperature in fired-clay bodies, Appl. Clay Sci. 163 (2018) 108–118. doi:10.1016/J.CLAY.2018.07.020.

[50] C. Coletti, G. Cultrone, L. Maritan, C. Mazzoli, Combined multi-analytical approach for study of pore system in bricks: How much porosity is there?, Mater. Charact. 121 (2016) 82–92. doi:10.1016/J.MATCHAR.2016.09.024.

[51] C. Coletti, G. Cultrone, L. Maritan, C. Mazzoli, How to face the new industrial challenge of compatible, sustainable brick production: Study of various types of commercially available bricks, Appl. Clay Sci. 124–125 (2016) 219–226. doi:10.1016/J.CLAY.2016.02.014.

[52] G. Cultrone, E. Sebastián, K. Elert, M.J. de la Torre, O. Cazalla, C. Rodriguez–Navarro, Influence of mineralogy and firing temperature on the porosity of bricks, J. Eur. Ceram. Soc. 24 (2004) 547–564. doi:10.1016/S0955-2219(03)00249-8.

[53] L. Graziani, E. Quagliarini, M. D’Orazio, Application of titania nanocoating to clay brick façades for biofouling prevention: efficiency and effect of substratum, Colloqui.AT.E. 1 (2014) 6.

[54] L. Graziani, E. Quagliarini, M. D’Orazio, Prevention of algal growth on clay façades by photocatalytic TiO2 nano- coating, (2015).

[55] L. Graziani, E. Quagliarini, F. Bondioli, M. D’Orazio, Durability of self-cleaning TiO2 coatings on fired clay brick façades: Effects of UV exposure and wet & dry cycles, Build. Environ. 71 (2014) 193–203. doi:10.1016/j.buildenv.2013.10.005.

[56] ASTM D4404-10. Standard test method for determination of pore volume and pore volume distribution of soil and rock by mercury intrusion porosimetry. American Society for Testing and Materials, (2010).

[57] UNI EN ISO 4287:2009. Geometrical Product Specifications (GPS) – Surface texture: Profile Method – Terms, Definitions and Surface Texture Parameters, International Standards Organization, (2009).

[58] T.H. Tran, N.D. Hoang, Estimation of algal colonization growth on mortar surface using a hybridization of machine learning and metaheuristic optimization, Sadhana - Acad. Proc. Eng. Sci. 42 (2017) 929–939. doi:10.1007/s12046-017-0652-6.

[59] J.H. Stock, M.W. Watson, Introduction to Econometrics, Third Edit, Pearson, 2015. http://library1.nida.ac.th/termpaper6/sd/2554/19755.pdf.

[60] W. Kong, S. Huang, F. Shi, J. Zhou, Y. Feng, Y. Xiao, Study on Microcystis aeruginosa growth in incubator experiments by combination of Logistic and Monod functions, Algal Res. 35 (2018) 602–612. doi:10.1016/J.ALGAL.2018.10.005.

[61] D.R. Tobergte, S. Curtis, Applied statistics using SSPS, Statistica, Matlab and R, Journal of Chemical Information and Modeling, 2013. doi:10.1017/CBO9781107415324.004.

Highlights

- An empirical failure model about microalgae biofouling was developed
- The model takes into account the main substrate properties influencing the growth
- It also considers the environmental temperature and relative humidity
- The model was developed and validated on fired bricks

An empirical failure model to predict biofouling growth on fired bricks due to microalgae

Enrico Quagliarini[a*], Benedetta Gregorini[a], Marco D'Orazio[a]

[a] Department of Construction, Civil Engineering and Architecture (DICEA), Università Politecnica delle Marche, via Brecce Bianche, 60131 Ancona, Italy

[*] Corresponding author, Tel: +39 07212204248.
Email addresses: e.quagliarini@staff.univpm.it (E. Quagliarini), b.gregorini@pm.univpm.it (B. Gregorini), m.dorazio@univpm.it (M. D'Orazio).

Highlights

- An empirical failure model about microalgae biofouling was developed
- The model takes into account the main substrate properties influencing the growth
- It also considers the environmental temperature and relative humidity
- The model was developed and validated on fired bricks

Abstract

The purpose of this study was to provide an empirical failure model predicting the microalgae growth on fired bricks surfaces. It was developed through a numerical fitting of experimental data present in literature. It considered the substrate properties related to biofouling (i.e. porosity and roughness) of different bricks under several environmental conditions (i.e. relative humidity and temperature). Results shows that the model is able to simulate the microalgae biofouling by explicitly taking into account such influencing factor. Finally, this empirical failure model is validated on a different dataset from literature and applied to time varying temperature.

Keywords: *microalgae biofouling; fired bricks; empirical failure model; substrate properties; environmental conditions;*

1 Introduction

When porous building materials are exposed to environmental weathering, their physicals and chemicals properties interact with biological factors, leading to changes in both its compositional and structural characteristics [1–3]. The growth process and vegetative development of organisms have a direct consequence on the material due to the metabolic activity connected with the growth of living organisms [4]. The living species that commonly dwell on these materials are ranging from microscopical bacterial cells to higher plants and animals [5].

Biofouling on porous building materials is a colonization process usually started by photoautotrophic microorganisms since they only need light, water and some inorganic components to start growing [1,2]. Among these, the most recurrent groups are green microalgae and cyanobacteria, shortly named as microalgae, and they usually develop in combination, especially in the European context [6–8]. Frequent maintenance and repairing interventions are then required in order to limit aesthetical, chemical and physical degradation they may produce: both ways, either repairing or not, could ultimately cause serious losses (economical or even cultural, if cultural heritage is involved) [9,10]. In order to describe and therefore limit microalgae biofouling risk on porous building materials, in recent years researchers adopted two strategies [11]: (1) determining and thus limiting, when possible, the influencing factors of biofouling growth; (2) providing models that can simulate and then forecast the biofouling risk.

Regarding the first one, literature works mainly focused on the factors that influenced the water activity: that is defined as the water available to microorganisms to growth [6,10,12–17]. They highlighted that a combination of environmental conditions, substrate properties and intrinsic aspects of the plumbing system of buildings (i.e. leaky parts and design defects of the construction) could ensure the growth and development of microalgae. For what concerns the environmental conditions, it was demonstrated that microalgae growth occurred only at saturation conditions [13,18], that is when water can be found at liquid state. From an engineering standpoint, however, two assumption can be done: water activity can be approximated with the relative humidity *RH*, as previously demonstrated in [19] and the saturation condition safety limit can be set for $RH \geq 98\%$ [18], even though brick surface could not be wet, and water activity is only present by capillary condensation [20]. Moreover, it was proved that temperature allows microalgae to develop between about 5°C and 40°C with an optimal growth condition at about 27.5°C [18,21,22]. Out of this range, microalgae growth process is unable to start or, if already started, it stops [1,2,18,23]. In this context, porosity and roughness were outlined as the main factors concerning the substrate properties [13,24–27]. In fact, roughness promotes the adherence of microalgae to the substrate while porosity is responsible for retaining water inside the material structure. Moreover, when the materials structure and geometry, in terms of porosity and roughness, is able to afford enough water activity for microalgae to start their growth, the chemical composition of the substrate may play only a secondary role, favouring or limiting their development [28–32].

For what concern the second strategy, literature has provided a reliable model for describing microalgae growth starting from experimental measures [33]. Based on the Avrami's theory, it connects the area covered by biofouling over the time by denoting a first phase of latency (when microalgae stains are not still visible), followed by a rapid growth, and finally a stagnation phase when the covered area reaches its maximum and becomes constant over the time. Such approach was applied to several type of porous buildings materials (i.e. mortars, fired bricks and stones), under different environmental conditions and biocides surface treatments, confirming its capabilities [18,26,33–35]. However, it never explicitly and quantitatively accounts for the growth influencing factors of the substrate and environmental conditions, as failure models usually do. This way, no failure models still exist in literature for microalgae growth on porous building materials, to the authors' knowledge, while numerous failure models have been presented for other type of biofouling (e. g. mould, fungi, actinomycetes) [19,36–43].

Hence, the aim of this work is to propose a first empirical microalgae growth failure model, that is able to explicitly take into account, for the first time, the main influencing factors of substrate parameters (such as porosity and roughness) and environmental conditions (such as temperature and relative humidity), as well as their variation over the time. Fired bricks are here considered due to the availability of a large set of experimental data in literature, but the methodology can be extended to other porous building materials when enough experimental data will be available. To this aim, this work is divided into three main phases. The first phase involves the definition of: the model general requirements (Section 2.1); the variables domains (Section 2.2) and the specific model equations (Section 2.3). The fitting method is then provided (Section 2.4). Lastly, resulting equations are presented and validated and the application of the model under time varying temperature is reported (Section 3).

2 Materials and methods

2.1 General requirements

As stated above, the starting point of this work is the modified Avrami's model [34,35] showed in (1):

$$X(t) = \frac{A_C}{A_T} \cdot (1 - \exp^{-K(t-t_1)^n}) \tag{1}$$

where the covered area by microalgae growth $X(t)$ [-] is given as a function of time t [day]. The final covered area ratio is represented by the parameter A_C/A_T which expresses the percentage of the covered area at the end of the process (A_C is the maximum covered area by biofouling on a specific sample, and A_T is the total area of the same sample), K [day^{-4}] is a rate parameter determined by the least squares method using experimental measurements. Lastly, the parameter t_1 represents the latency time [day] before a chromatic variation occurs on the material surface and the coefficient n is the Avrami's coefficient which can be assumed equal to 4 [34].

The model variables are chosen according to literature findings. Porosity P [-] and roughness R [μm] are the main factors characterising the substrate [6,25,26] and, their values are easily measurable and available in literature (see Section 2.2). Temperature T [°C] and relative humidity RH [%] are instead selected as the main factors representing environmental conditions [13,14,18].

In this way:

- since literature showed that, regardless of the temperature, RH determines the actual possibility for microalgae to growth, according to which growth happens only if $RH \geq 98\%$ [18], it can be considered as an on/off factor;

- when $RH \geq 98\%$ and $5°C \leq T \leq 40°C$ growth can happen depending on T, P and R, otherwise it cannot [13,18];
- thus, P, R and T directly affect the microalgae coverage X through its parameters A_C/A_T, K and t_1 [18,26,34,35].

Inorganic compounds are here not directly considered due to their difficult measurement and their possible non-homogeneous distribution, but they are assumed as available. At the same time, an optimal day/night period is assumed to consider the influence of the light. These come from the choice of the experimental dataset (see Section 2.2). Both these assumptions can be considered as conservative standpoints.

Equation (2) shows the analytical translation of the previous requirements.

$$X(T,RH,P,R,t) = \Omega(RH) \cdot \frac{A_C}{A_T}(T,P,R) \cdot \left[1 - \exp^{-K(T,P,R)\cdot\left(t - t_1(T,P,R)\right)^4}\right] \quad (2)$$

where the $\Omega(RH)$ is defined as in (3) and $5°C \leq T \leq 40°C$.

$$\Omega(RH) = \begin{cases} 0, & RH < 98\% \\ 1, & RH \geq 98\% \end{cases} \quad (3)$$

Besides, two analytical requirements over the time t can be stated, as reported in (4).

$$\begin{cases} X(t) = 0, \forall t < t_1(T,P,R) \\ X(t_i) \leq X(t_{i+1}), \forall t_i < t_{i+1} \end{cases} \quad (4)$$

The first one involves the latency time t_1 and it tries to overcome an analytical inaccuracy. In fact, the use of t_1 can lead to a miscalculation on the covered area: since the function is even, when the latency time is different from 0, the covered area at t=0 is higher than 0 with a decreasing trend between t = 0 and t = t_1. This means that the growth curve minimum is equal to 0 when t= t_1, too. This is not so correct from a physical description of microalgae growth, even if t_1 is usually very short if compared to the total growth time and the predicted biofouling coverage in this interval is rather poor. Thus, microalgae growth is set to be 0 until the latency time is reached. The second condition states that the model has to be a monotonically not decreasing function, that is, the reached covered area can be constant or it can increase, according to the environmental conditions. In fact, previous researches showed that, once settled, microalgae are able to retain water inside them and therefore survive i.e. dry periods [2,44].

2.2 The experimental dataset and domains determination

For the experimental dataset based on fired brick substrates, no novel experimental tests are performed, but a very large dataset coming from a previous work [18] is used. This dataset is in fact: (1) comparable to other ones of previous failure model used in literature [19,39,45,46] and (2) representative of the main influencing growing factors for microalgae, such as *P* and *R*. Moreover, it considers two of the most recurrent species of microalgae on building materials [6], namely *Chlorella mirabilis* (green microalga) and *Chroococcidiopsis fissurarum* (cyanobacterium), by accounting for them an optimal day/night period equal to 14/10 h respectively[18] and an adequate level of inorganic compound, according to ASTM D5589-09 standard method [47].

Table 1 summarizes the substrate properties (*P* and *R*) of the five fired bricks (SP_1, …, SP_5), and the seven different environmental combinations of *T* and *RH* (EC_1, …, EC_7).

Table 1. Combination of the tested substrate properties (SP) and environmental conditions (EC) [18]. Three samples were tested for each substrate property (SP).

	Substrate Properties		**Environmental Conditions** Temperature [°C] – Relative humidity [%]						
	Porosity [-]	Roughness [µm]	EC_1	EC_2	EC_3	EC_4	EC_5	EC_6	EC_7
SP_1	0.19	4.50	T=27.5 RH=75	T=27.5 RH=87	T=27.5 RH=98	T=5 RH≈100	T=10 RH≈100	T=27.5°C RH≈100	T=40 RH≈100
SP_2	0.19	5.54							
SP_3	0.25	2.95							
SP_4	0.44	6.60							
SP_5	0.44	7.60							

Materials SP_1, SP_3 and SP_5 are considered for the fitting process since they are comprehensive of the substrate domain, representing the minimum, maximum and intermediate values for both *P* and *R*. On the other hand, SP_2 and SP_4 are used in the post fitting process in order to validate its results. All the tested environmental conditions are taken into account in the fitting process. Hence, the dataset for the experimental fitting process is composed by 63 experimental microalgae growth curves, referring to 3 samples for 3 substrates under 7 different environmental conditions and by 42 curves for the validation step.

Common P and R values of fired bricks were also investigated [25–27,29,35,48–54] to see how the experimental data set (Table 1) is representative. This way, an application range for the empirical failure model can be provided. The review described 60 different brick porosity and 20 roughness values, respectively (Figure 1). It is worth noting that the (open) porosity and the roughness, usually considered in literature [25,27,29,35,48,54,55] as microalgae growing factors, are those determined according to the ASTM D4404-10 standard [56] and UNI EN ISO 4287:2009 standard[1] [57], respectively. We will refer to such references in the following.

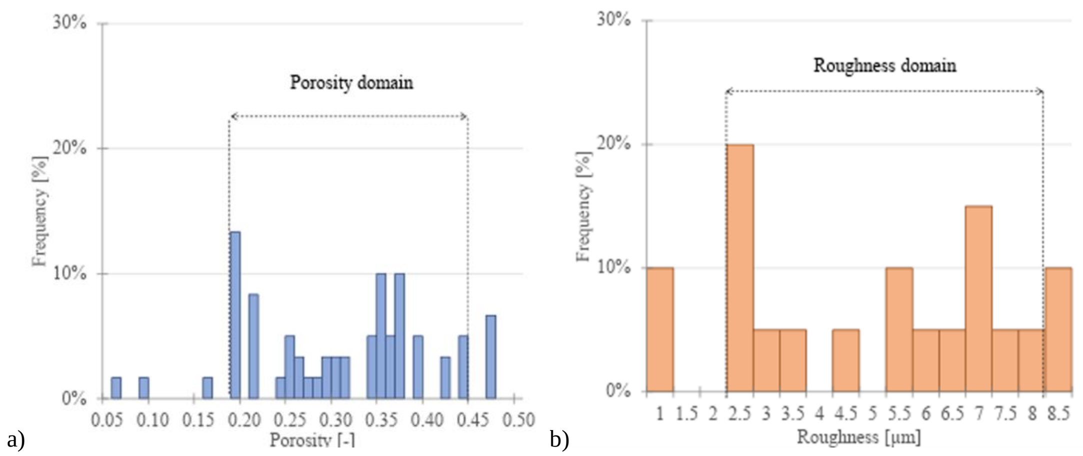

Figure 1. Comparison between porosity and roughness values from literature [25–27,29,35,48–54] and the porosity and roughness domain from the selected database [18].

By comparing the literature review results and the experimental dataset reported in Table 1, the domain for P and R is set as reported in (5).

$$\begin{cases} 0.19 \le P \le 0.44 \\ 2.50\mu m \le R \le 8.00\mu m \end{cases} \quad (5)$$

In particular, it is worth noting that the porosity domain set for the model includes 87% samples' values, while the roughness domain covers 80% of samples provided by literature.

2.3 *Experimental trend and analytical model definition*

Figure 2 shows the experimental trend of the parameter A_C/A_T, K and t_1 obtained from the used dataset: the parameter values refer to the specimens of the tested materials (SP_1, SP_3 and SP_5) under saturation condition (as reported in EC_4, …, EC_7), for a total of 36 experimental data for each parameter. In the between of domain, T

[1] Roughness values were determined according to R_a calculation.

predominantly influences A_C/A_T and K, determining an increasing trend from 5°C to about 27.5°C and a decreasing one from about 27.5°C to 40°C. These trends hold for each P and R. Lastly, in Figure 2 (c) the latency time t_1 shows a constant trend not depending on temperature, conversely, it is influenced by P and R.

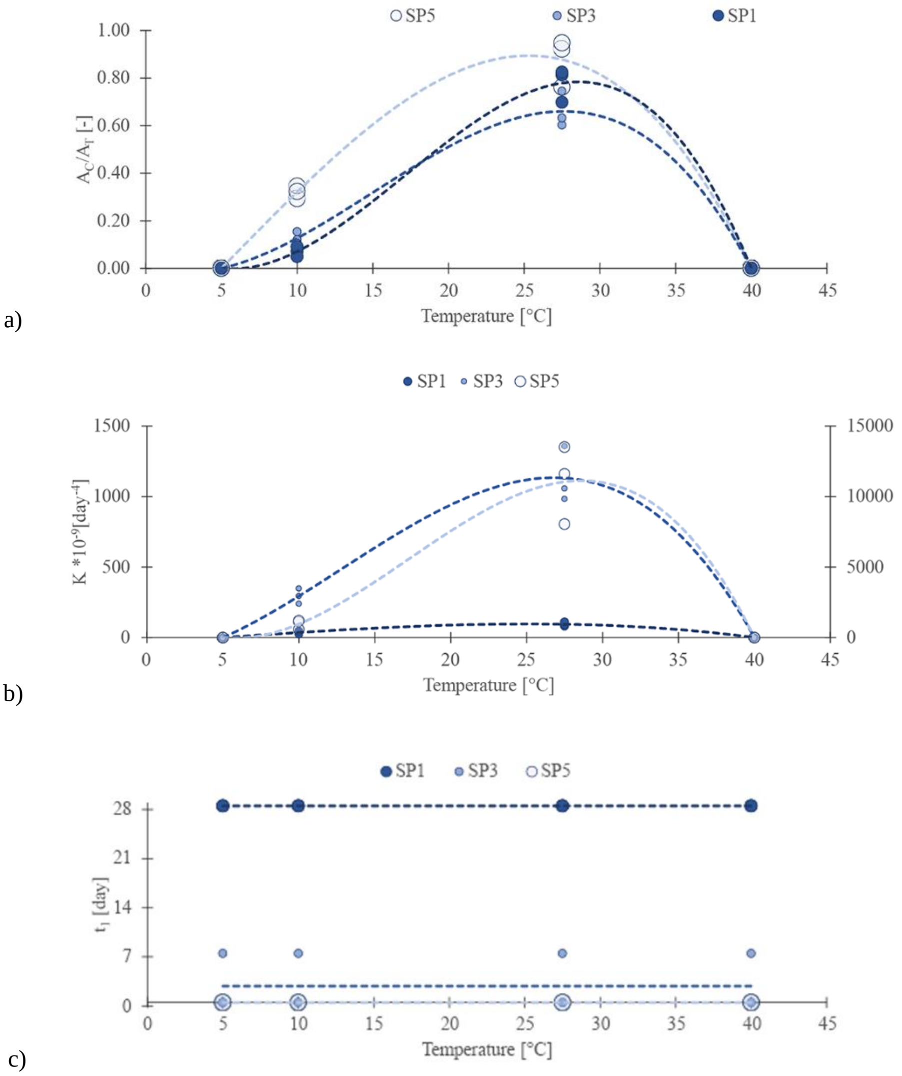

Figure 2. Experimental trend of bricks parameters: (a) A_C/A_T parameter; (b) K parameter; (c) t_1 parameter. The graphs are reported according to the temperature domain. The blue scale (dark-light) indicates the increasing porosity; the increasing dimension of the spot indicates the increasing roughness value. In (b) two y-axis were used since the K parameters are significantly different: SP_1 and SP_3 refer to the left y-axis, SP_5 refers to the right y-axis.

In this way, aiming at determining the simplest possible model, having only 4 different temperature values, a 3rd degree polynomial is set in order to describe A_C/A_T and K as functions of T, having its coefficients depending on P and R. For the t_1 parameter, a constant coefficient depending only on P and R is set. The above observations are reported in (6):

$$\begin{cases} \frac{A_C}{A_T}(T,P,R) = c_{0,A}(P,R) + c_{1,A}(P,R)\cdot T + c_{2,A}(P,R)\cdot T^2 + c_{3,A}(P,R)\cdot T^3 \\ K(T,P,R) = c_{0,K}(P,R) + c_{1,K}(P,R)\cdot T + c_{2,K}(P,R)\cdot T^2 + c_{3,K}(P,R)\cdot T^3 \\ t_1(P,R) = c_{0,t}(P,R) \end{cases} \quad (6)$$

where the coefficients reported in (6) result from the fitting process (see Section 2.4).

Finally, the codomains of each involved parameter are reported in equation (7):

$$\begin{cases} 0 \le \frac{A_C}{A_T}(T,P,R) \le 1 \\ K(T,P,R) \ge 0 \\ t_1(P,R) \ge 0 \end{cases} \quad , \ \forall T \in [5;40], \forall P \in [0.19;0.44], \forall R \in [2.50;8.00] \quad (7)$$

2.4 The fitting process

From condition (6), a linear system of the temperature coefficient can be set as in (8).

$$\begin{cases} c_{n,A} = \alpha_{n,1,A} F_{1,A}(P,R) + \alpha_{n,2,A} F_{2,A}(P,R) + \alpha_{n,3,A} F_{3,A}(P,R) \\ c_{n,K} = \alpha_{n,1,K} F_{1,K}(P,R) + \alpha_{n,2,K} F_{2,K}(P,R) + \alpha_{n,3,K} F_{3,K}(P,R), \quad n = 0,...,3 \\ c_{0,t} = \alpha_{0,1,t} F_{1,t}(P,R) + \alpha_{n,2,t} F_{2,t}(P,R) + \alpha_{n,3,t} F_{3,t}(P,R) \end{cases} \quad (8)$$

The $F_1,\ldots, F_3$ considered the effect of *P* and *R* values and they are defined in (9)

$$\begin{cases} F_1(P,R) \in \{P^{j_1}, R^{k_1}, 0\} \\ F_2(P,R) \in \{P^{j_2}, R^{k_2}, 0\}, \quad j_1,..., j_3, k_1,..., k_3 \in \mathbb{Z} \\ F_3(P,R) \in \{P^{j_3}, R^{k_3}, 0\} \end{cases} \quad (9)$$

This means that the combination of $F_1,\ldots, F_3$ can consider only *P* element, conversely only *R* elements, it may be resumed in a constant value (e.g. for *j* and *k* exponent resulting equal to 0) or even it can result equal to 0. This is due because the trends for both *P* and *R* were not clearly obtainable from the experimental evidences [18], and therefore determined in advanced as for temperature.

Hence, once set conditions (8)-(9), the fitting process is iteratively run by determining the α values and the right combination of $F_1, \ldots, F_3$ for the three parameters, following what is reported in (10) where $F_1, \ldots, F_3$ have the same degree for each surface properties SP.

$$\begin{cases} \left|\begin{matrix} \alpha_{0,1} & \alpha_{0,2} & \alpha_{0,3} \\ \alpha_{1,1} & \alpha_{1,2} & \alpha_{1,3} \\ \alpha_{2,1} & \alpha_{2,2} & \alpha_{2,3} \\ \alpha_{3,1} & \alpha_{3,2} & \alpha_{3,3} \end{matrix}\right| \left|\begin{matrix} F_1(P,R) \\ F_2(P,R) \\ F_3(P,R) \end{matrix}\right|_{SP1} = \left|\begin{matrix} c_0 \\ c_1 \\ c_2 \\ c_3 \end{matrix}\right|_{SP1} \\ \left|\begin{matrix} \alpha_{0,1} & \alpha_{0,2} & \alpha_{0,3} \\ \alpha_{1,1} & \alpha_{1,2} & \alpha_{1,3} \\ \alpha_{2,1} & \alpha_{2,2} & \alpha_{2,3} \\ \alpha_{3,1} & \alpha_{3,2} & \alpha_{3,3} \end{matrix}\right| \left|\begin{matrix} F_1(P,R) \\ F_2(P,R) \\ F_3(P,R) \end{matrix}\right|_{SP3} = \left|\begin{matrix} c_0 \\ c_1 \\ c_2 \\ c_3 \end{matrix}\right|_{SP3} \\ \left|\begin{matrix} \alpha_{0,1} & \alpha_{0,2} & \alpha_{0,3} \\ \alpha_{1,1} & \alpha_{1,2} & \alpha_{1,3} \\ \alpha_{2,1} & \alpha_{2,2} & \alpha_{2,3} \\ \alpha_{3,1} & \alpha_{3,2} & \alpha_{3,3} \end{matrix}\right| \left|\begin{matrix} F_1(P,R) \\ F_2(P,R) \\ F_3(P,R) \end{matrix}\right|_{SP5} = \left|\begin{matrix} c_0 \\ c_1 \\ c_2 \\ c_3 \end{matrix}\right|_{SP5} \end{cases} \tag{10}$$

The process stops when the following two requirements are achieved. The first requirement verifies the analytical correctness of the model by determining the adjusted coefficient of determination R^2_{adj} since a multiple variable regression is considered. The calculation of R^2_{adj} is shown in equation (11) and all the R^2_{adj} have to be higher than 0.85. Such limit was previously adopted in other models to consider the accuracy of the fitting good [58–60].

$$R^2_{adj} = 1 - \frac{RSS}{TSS} \cdot \frac{n-1}{n-p-1} \geq 0.85 \tag{11}$$

The *RSS* is the residual sum of squares between the experimental and the fitted data, *TSS* is the total sum of squares of the differences between the experimental data and its mean, *n* is the number of observation and *p* is the total number of explanatory variables in the model [61].

Subsequently, the second requirement involves the experimental correctness of the model. It is satisfied when conditions reported in (12) are fulfilled.

$$\begin{cases} \min\left[\dfrac{A_C}{A_T}_{\text{exp}}\right] \le \dfrac{A_C}{A_T}(T,P,R) \le \max\left[\dfrac{A_C}{A_T}_{\text{exp}}\right] \\ \min\left[K_{\text{exp}}\right] \le K(T,P,R) \le \max\left[K_{\text{exp}}\right] \\ \min\left[t_{1,\text{exp}}\right] \le t_1(P,R) \le \max\left[t_{1,\text{exp}}\right] \end{cases} \tag{12}$$

After having defined all the parameters with their coefficients, the failure model is tested on SP_2 and SP_4 so as to have a first validation, following the same criteria: R^2_{adj} still has to be higher than 0.85, as analytical requirement and the experimental correctness must be verified by conditions reported in (12).

3 Results

3.1 The failure model for bricks

Condition (13) summarise the resulting α values and the combinations of $F_1, \dots, F_3$ of each parameter, by also resuming condition (6) for the temperature equations.

$$
\begin{cases}
\dfrac{A_C}{A_T}(T,P,R)=\left|\begin{matrix}
-3.419[-] & 9.2\cdot 10^{-2}\left[\dfrac{1}{\mu m}\right] & -5.7\cdot 10^{-3}\left[\dfrac{1}{\mu m^2}\right] \\
8.798\cdot 10^{-1}\left[\dfrac{1}{°C}\right] & -3.1032\cdot 10^{-2}\left[\dfrac{1}{\mu m\cdot °C}\right] & 2.16\cdot 10^{-3}\left[\dfrac{1}{\mu m^2\cdot °C}\right] \\
-3.98\cdot 10^{-2}\left[\dfrac{1}{°C^2}\right] & 2.8023\cdot 10^{-3}\left[\dfrac{1}{\mu m\cdot °C^2}\right] & -2.184\cdot 10^{-4}\left[\dfrac{1}{\mu m^2\cdot °C^2}\right] \\
5\cdot 10^{-4}\left[\dfrac{1}{°C^3}\right] & -5.21\cdot 10^{-5}\left[\dfrac{1}{\mu m\cdot °C^3}\right] & 4.198\cdot 10^{-6}\left[\dfrac{1}{\mu m^2\cdot °C^3}\right]
\end{matrix}\right|\left|\begin{matrix} P^2 \\ R \\ R^2 \end{matrix}\right|\cdot\left|\begin{matrix} T^0 \\ T^1 \\ T^2 \\ T^3 \end{matrix}\right| \\
K(T,P,R)=\left|\begin{matrix}
-1.018137\cdot 10^{-6}\left[day^{-4}\right] & 2.638435\cdot 10^{-5}\left[day^{-4}\right] & -1.109344\cdot 10^{-3}\left[\mu m^8\cdot day^{-4}\right] \\
3.832828\cdot 10^{-7}\left[\dfrac{day^{-4}}{°C}\right] & -1.056712\cdot 10^{-5}\left[\dfrac{day^{-4}}{°C}\right] & 2.729806\cdot 10^{-4}\left[\dfrac{\mu m^8\cdot day^{-4}}{°C}\right] \\
-3.978387\cdot 10^{-8}\left[\dfrac{day^{-4}}{°C^2}\right] & 1.173803\cdot 10^{-6}\left[\dfrac{day^{-4}}{°C^2}\right] & -1.081282\cdot 10^{-5}\left[\dfrac{\mu m^8\cdot day^{-4}}{°C^2}\right] \\
7.709831\cdot 10^{-10}\left[\dfrac{day^{-4}}{°C^3}\right] & -2.315303\cdot 10^{-8}\left[\dfrac{day^{-4}}{°C^3}\right] & 1.169671\cdot 10^{-7}\left[\dfrac{\mu m^8\cdot day^{-4}}{°C^3}\right]
\end{matrix}\right|\left|\begin{matrix} P \\ P^3 \\ R^{-8} \end{matrix}\right|\cdot\left|\begin{matrix} T^0 \\ T^1 \\ T^2 \\ T^3 \end{matrix}\right| \\
t_1(P,R)=\left|\begin{matrix} 4.73\cdot 10^{-5}[day] & -2.88\cdot 10^{-4}\left[\dfrac{day}{\mu m}\right] & -2.66\cdot 10^{-4}\left[\dfrac{day}{\mu m^2}\right] \end{matrix}\right|\left|\begin{matrix} P^{-8} \\ R \\ R^2 \end{matrix}\right|
\end{cases}
\qquad (13)
$$

Figure 3 shows that all the R^2_{adj} are higher than 0.85 for A_C/A_T, K and t_1.

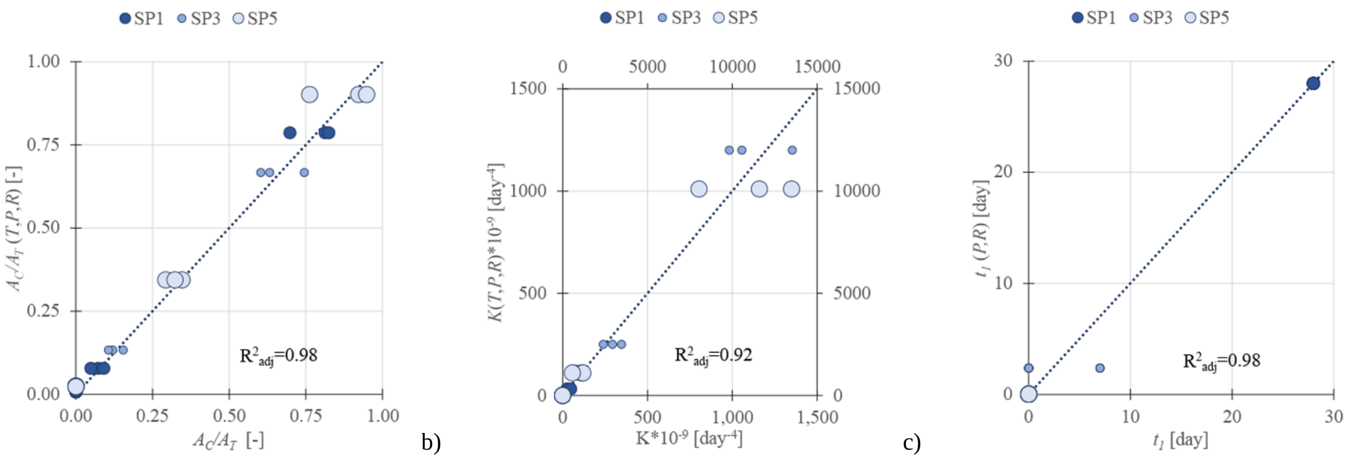

a) b) c)

Figure 3. Coefficient of determination R^2 of the parameter. (a) A_C/A_T parameters; (b) K parameter; (c) t_1 parameter. The blue scale (dark-light) indicates the increasing porosity the increasing dimension of the spot indicates the increasing roughness value. In (b) two y-axis were used since the K parameters are significantly different: SP_1 and SP_3 refer to the left y-axis, SP_5 refers to the right y-axis.

Lasty, both the experimental values and the fitted curves are reported in Figure 4. These last ones falls within the experimental values, verifing the condition proposed in (12).

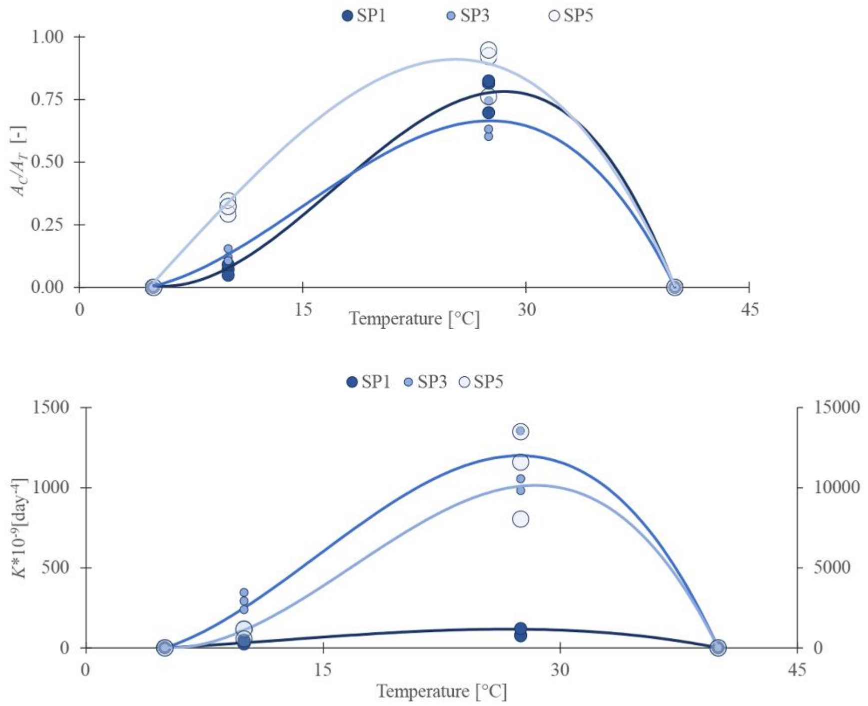

a)

b)

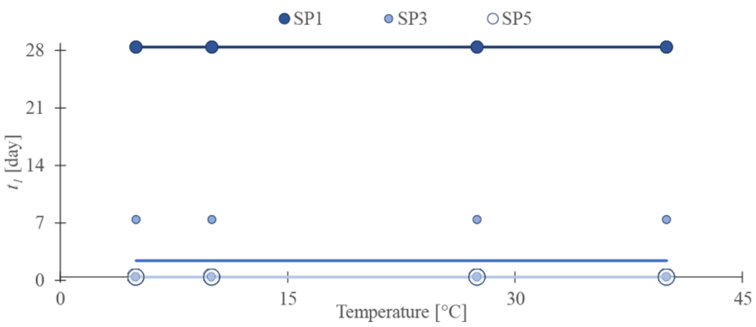

c)

Figure 4. Comparison between the the experimental values and the fitted curves for the sufaces properties SP_1 SP_3 and SP_5: (a) A_C/A_T (b) K and (c) t_1. The blue scale (dark-light) indicates the increasing porosity; the increasing dimension of the spot indicates the increasing roughness value. In (b) two y-axis were used since the K parameters are significantly different: SP_1 SP_3 refer to the left y-axis, SP_5 refers to the right y-axis.

3.2 Failure model validation

The failure model is then applied on the second dataset. As shown in Figure 5, the three R^2_{adj} were always higher than 0.85.

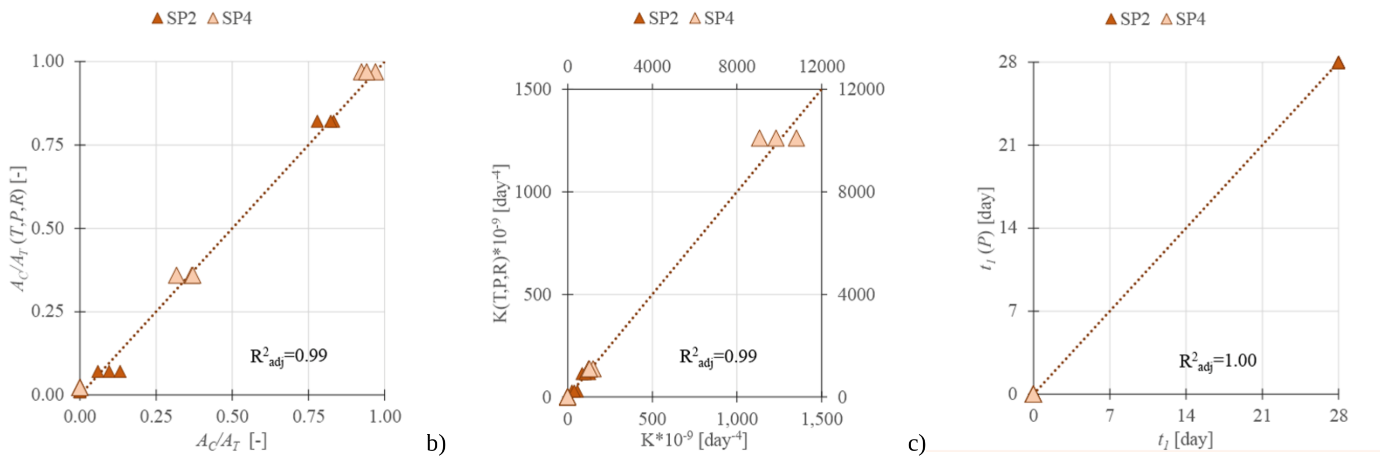

a) b) c)

Figure 5. Coefficient of determination R^2 of the parameters. (a) A_C/A_T parameters; (b) K parameter; (c) t_1 parameter. The red scale (dark-light) indicates the increasing porosity; the increasing dimension of the spot indicates the increasing roughness value. In (b) two y-axis were used since the K parameters are significantly different: SP_2 refer to the left y-axis, SP_4 refers to the right y-axis.

Figure 6, instead, shows that the curves determined by the failure model fell within the range of their respective experimental data.

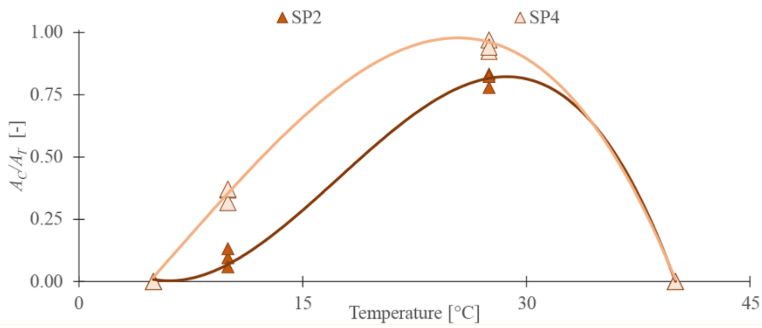

a)

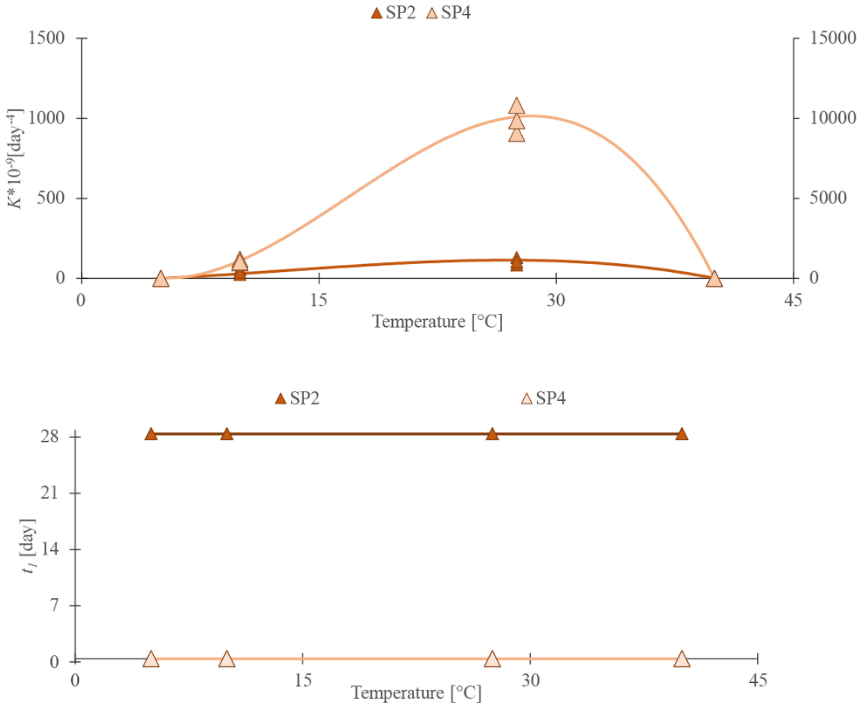

b)

c)

Figure 6. Comparison between the the experimental values and the fitted curves for the sufaces properties SP_2 and SP_4: (a) A_C/A_T (b) K and (c) t_I. The dotted red lines indicate the minimum and maximum curve for P and R values. The red scale (dark-light) indicates the increasing porosity; the dimension of the spot (6-7) indicates the roughness value. In (b) two y-axis were used since the K parameters are significantly different: SP_2 refers to the left y-axis, SP_4 refers to the right y-axis.

As a last qualitative validation step, according to other previous model validation [39,46], the curves describing microalgae growth $X(t, T, RH, P, R)$ are determined for the validation substrates SP_2 and SP_4 under the tested environmental condition EC_5 and EC_6 (Table 1) and overlapped to the experimental data obtained in [18]. All the curves well fit the experimental values (Figure 7).

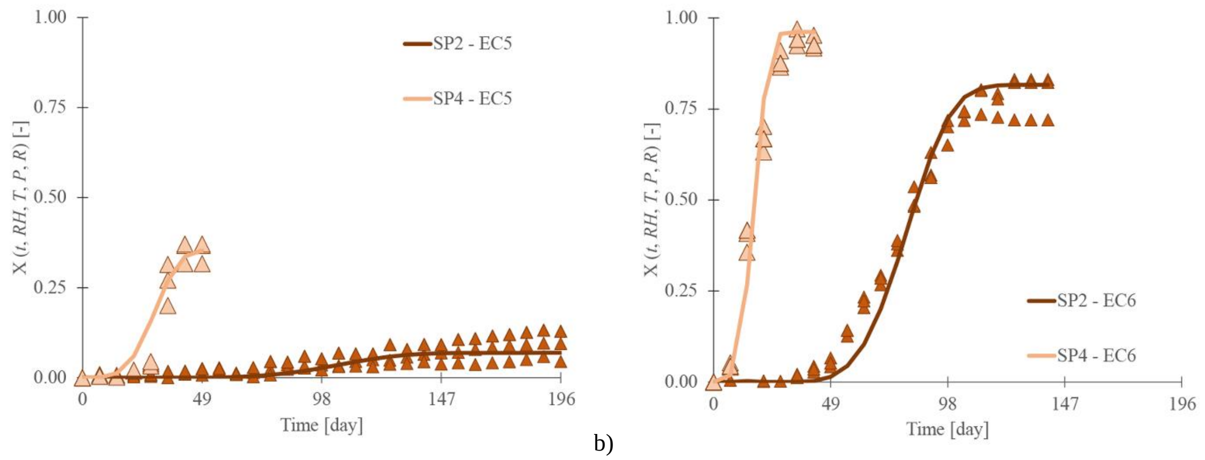

a) b)

Figure 7. Comparison of the covered area X(t, T, RH, P, R) obtained with the failure model and experimental data for SP_2, and SP_4 [18]:a) when exposed to EC_5;b) when exposed to EC_6. Lines indicate the failure model curves; points indicate the experimental data.

3.3 *Failure model application over time-variable environmental conditions*

Lastly, this paragraph shows the model application for a representative brick substrate exposed to time-variable environmental conditions (Table 2).

Table 2**.** Specification for the model application.

Material		Condition (C)		
Porosity [-]	Roughness [µm]	n°	Temperature [°C]	Exposure Time [day]
0.19	2.75µm	1	14	50
		2	7.5	50
		3	20	50
		4	27.5	50

The brick properties are chosen in order to describe the most recurrent ones according to Figure 1. The assumed four conditions do not simulate a real dataset, but they allow improving the readability of the combination process. In particular, the gradient between the four temperatures values allows having four distinctive branches that significantly differ from each other and the exposure time of 50 days led the growth process for each condition be clearly recognizable. Lastly, time and the time dependent variable (*T* and *RH*) are daily discretized and kept constant during the day for sake of simplicity.

The combination of the branches over the time is made by following these 2 assumptions: (1) *P* and *R* are given and they both cannot change; (2) the coverage cannot go back and decrease, as already stated in equation (4). Hence, each involved *n*-branch of each *T*-dependent curve is joined to another *n+1*-curve by simply determining the time shift $t_{s,n}$ following simple steps from equation as reported in equation (14):

$$t_{s,n} = +\sqrt[4]{-\left(\frac{1}{K(T_{n+1})}\right)\cdot \ln\left(1-\frac{X_n}{\frac{A_C}{A_T}(T_{n+1})}\right)} - t + t_1 \qquad (14)$$

The logarithmic calculation is possible only if the reached covered area X_n is lower than the A_C/A_T (T_{n+1}), otherwise the covered area is kept constant over the time.

Figure 8. shows the graphical combination of such branches and the resulting curve under time variable environmental conditions. In Figure 8. (a), the *T*-curves are determined and each branch for the corresponding exposure time is selected. Since the covered area of C_1 ($X_{n=1}$) is higher than the A_C/A_T ($T_{n=2}$), the latency time is not determined, and hence, for all the C_2 exposure time the covered area is maintained constant. Figure 8. (b) shows the resulting combination of the branches for C_1, C_3 and C_4 and the constant growth curve for T=7.5°C.

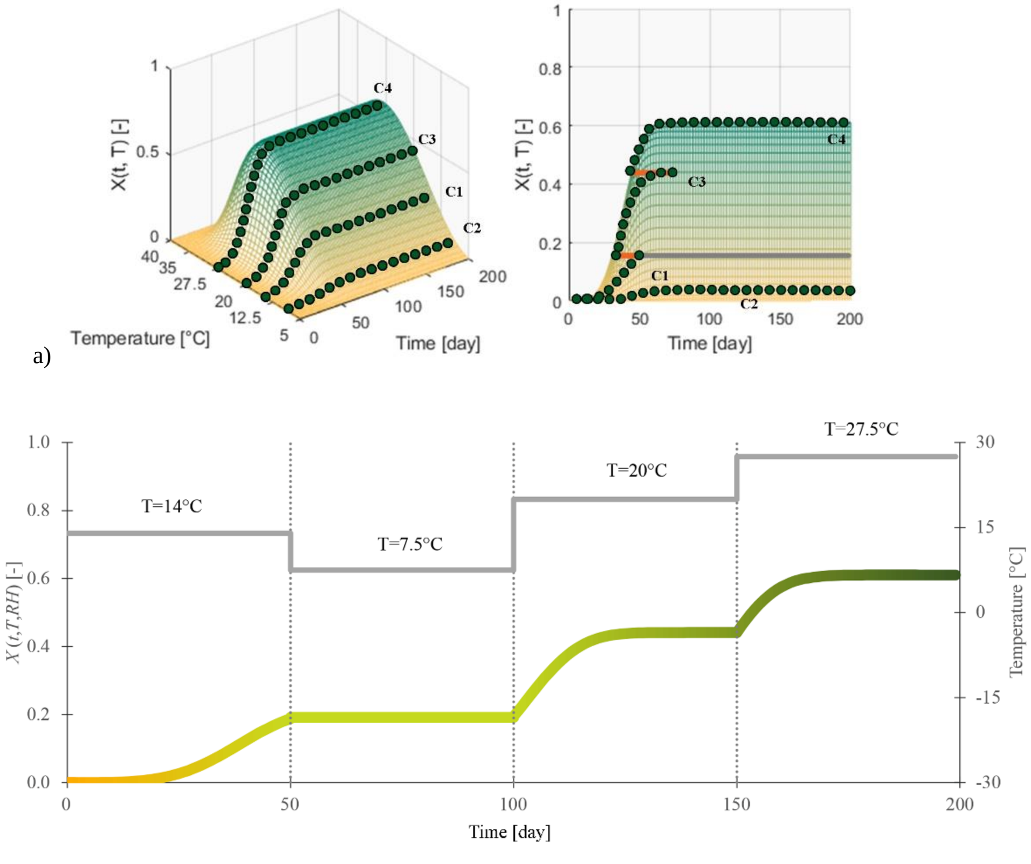

Figure 8. Application of the model to time changing environmental conditions: a) combination methods; b) resulting curve for temperature variation over time. In (a) the covered area is following the colour scale green-yellow resembling microalgae biofouling effect; dots represent the selected curve; lines orange indicate the combination effect of the time shift; line grey indicates that it was not possible to determine the time shift; in (b) the colour scale yellow green is maintained for the total microalgae curve.

4 Conclusion

Failure models for biofouling on building materials are becoming a more and more unavoidable need: by making quantitative predictions, they can assist professionals and researchers in developing guidelines for interventions leading to a decrease in maintenance costs. Literature have already provided such models for mould and fungi growth, but it is still limited for microalgae growth. This work tries to fill this gap by presenting a novel empirical failure model for fired bricks by taking into account the main substrate and environmental parameters influencing such growth, which are porosity and roughness, as well as temperature and relative humidity. It starts from the modified Avrami's model, by determining its three main parameters from experimental results, by also improving it about some miscalculations in the range of the latency time. From the obtained results, it is evident that such model is analytically intuitive and easy to implement. From an engineering standpoint, the novel empirical model seems to be generally applicable since the tested domain of porosity and roughness covers more than 80% of the fired bricks reported in literature. Finally, the application of such model considering time variable environmental conditions is proposed too.

Future works should consider more brick type and different environmental conditions as soon as experimental data will be available. Once confirmed its correctness for bricks, the model application could be extended to other porous building materials (such as i.e. stones, plasters and mortars) prone to microalgae growth. Moreover, thanks to its ability of considering time varying environmental conditions the model could be implemented on heat and moisture simulation software, as it is already happening for other biofouling models. This will lead to the application of the failure model to a real weather dataset, even considering the water content of the substrate instead of solely relative humidity.

Acknowledgements

This research did not receive any specific grant from funding agencies in the public, commercial, or not-for-profit sectors.

Nomenclature

Experimental parameters by literature researches (based on modified Avrami's Theory)	
X	covered area by microalgae biofouling [-]
A_C/A_T	parameter of final covered area ratio [-]
K	parameter of growth rate [day^{-4}]
t_1	parameter of latency time [day]
Fitted parameters (failure model)	
$X(t, T, RH, P, R)$	covered area by microalgae biofouling [-]
$A_C/A_T\ (T, P, R)$	parameter of final covered area ratio [-]
$K\ (T, P, R)$	parameter of growth rate [day^{-4}]
$t_1\ (P, R)$	parameter of latency time [day]
$\Omega(RH)$	on off parameter for relative humidity [-]
Variables	
t	time [day]
T	temperature [°C]
RH	relative humidity [%]
P	total porosity [%]
R	roughness [μm]
Coefficients	
c	temperature equation coefficient
α	coefficient for material properties
F	element describing the effect of P or R
Subscript and Superscript	
n	number of temperature coefficients, from 0 to 3
$_{1,2,3}$	number of material coefficient for both α and F values

n_j	number of coefficient/exponents for porosity
n_k	number of coefficient/exponents for roughness

References

[1] P. Tiano, Biodegradation of Cultural Heritage: Decay Mechanisms and Control Methods, 9th ARIADNE Work. “Historic Mater. Their Diagnostic.” (2002) 1–37. doi:10.1.1.129.3386.

[2] G. Caneva, M.P. Nugari, O. Salvadori, Biology in the Conservation of Works of Art, ICCROM, 1991.

[3] C. Ferrari, G. Santunione, A. Libbra, A. Muscio, E. Sgarbi, C. Siligardi, G.S. Barozzi, Review on the influence of biological deterioration on the surface properties of building materials: Organisms, materials, and methods, Int. J. Des. Nat. Ecodynamics. 10 (2015) 21–39. doi:10.2495/DNE-V10-N1-21-39.

[4] O. Guillitte, Bioreceptivity: a new concept for building ecology studies, Sci. Total Environ. 167 (1995) 215–220. doi:10.1016/0048-9697(95)04582-L.

[5] T. Warscheid, J. Braams, Biodeterioration of stone: a review, Int. Biodeterior. Biodegradation. 46 (2000) 343–368. doi:10.1016/S0964-8305(00)00109-8.

[6] H. Barberousse, B. Ruot, C. Yéprémian, G. Boulon, An assessment of façade coatings against colonisation by aerial algae and cyanobacteria, Build. Environ. 42 (2007) 2555–2561. doi:10.1016/j.buildenv.2006.07.031.

[7] M.L. Coutinho, A.Z. Miller, M.F. Macedo, Biological colonization and biodeterioration of architectural ceramic materials: An overview, J. Cult. Herit. 16 (2015) 759–777. doi:10.1016/j.culher.2015.01.006.

[8] C.C. Gaylarde, P.M. Gaylarde, A comparative study of the major microbial biomass of biofilms on exteriors of buildings in Europe and Latin America, Int. Biodeterior. Biodegrad. 55 (2005) 131–139. doi:10.1016/j.ibiod.2004.10.001.

[9] C. Gaylarde, M. Ribas Silva, T. Warscheid, Microbial impact on building materials: an overview, Mater. Struct. 36 (2003) 342–352. doi:10.1007/BF02480875.

[10] I. Flores-Colen, J. de Brito, V.P. de Freitas, Stains in facades’ rendering - Diagnosis and maintenance techniques’ classification, Constr. Build. Mater. 22 (2008) 211–221. doi:10.1016/j.conbuildmat.2006.08.023.

[11] T. Verdier, M. Coutand, A. Bertron, C. Roques, A review of indoor microbial growth across building

materials and sampling and analysis methods, Build. Environ. 80 (2014) 136–149. doi:10.1016/J.BUILDENV.2014.05.030.

[12] P. Johansson, Determination of the Critical Moisture Level for Mould Growth on Building Materials, 2014.

[13] D. Giovannacci, C. Leclaire, M. Horgnies, M. Ellmer, J.D. Mertz, G. Orial, J. Chen, F. Bousta, Algal colonization kinetics on roofing and façade tiles: Influence of physical parameters, Constr. Build. Mater. 48 (2013) 670–676. doi:10.1016/j.conbuildmat.2013.07.034.

[14] H. Barberousse, R.J. Lombardo, G. Tell, A. Couté, Factors involved in the colonisation of building façades by algae and cyanobacteria in France, Biofouling. 22 (2006) 69–77. doi:10.1080/08927010600564712.

[15] O. Guillitte, R. Dreesen, Laboratory chamber studies and petrographical analysis as bioreceptivity assessment tools of building materials, Sci. Total Environ. 167 (1995) 365–374. doi:10.1016/0048-9697(95)04596-S.

[16] F. Gladis, R. Schumann, Influence of material properties and photocatalysis on phototrophic growth in multi-year roof weathering, Int. Biodeterior. Biodegradation. 65 (2011) 36–44. doi:10.1016/J.IBIOD.2010.05.014.

[17] C.A. Crispim, P.M. Gaylarde, C.C. Gaylarde, Algal and cyanobacterial biofilms on calcareous historic buildings, Curr. Microbiol. 46 (2003) 79–82. doi:10.1007/s00284-002-3815-5.

[18] E. Quagliarini, A. Gianangeli, M. D'Orazio, B. Gregorini, A. Osimani, L. Aquilanti, F. Clementi, Effect of temperature and relative humidity on algae biofouling on different fired brick surfaces, Constr. Build. Mater. 199 (2019) 396–405. doi:10.1016/J.CONBUILDMAT.2018.12.023.

[19] A. Hukka, H. Viitanen, A mathematical model of mould growth on wooden material, Wood Sci. Technol. 33 (1999) 475–485. doi:10.1007/s002260050131.

[20] A. Stazi, M. D'Orazio, E. Quagliarini, In-life prediction of hygrometric behaviour of buildings materials: an application of fractal geometry to the determination of adsorption and suction properties, Build. Environ. 37 (2002) 733–739. doi:10.1016/S0360-1323(01)00064-6.

[21] J.A. Raven, R.J. Geider, Temperature and algal growth, New Phytol. 110 (1988) 441–461.

doi:10.1111/j.1469-8137.1988.tb00282.x.

[22] K. Lengsfeld, M. Krus, Microorganism on façades – reasons, consequences and measures, (2001) 0–7.

[23] A. Konopka, T.D. Brock, Effect of temperature on blue-green algae (Cyanobacteria) in Lake Mendota, Appl. Environ. Microbiol. 36 (1978) 572–576. doi:10.1520/C1421-10.2.

[24] T.H. Tran, A. Govin, R. Guyonnet, P. Grosseau, C. Lors, E. Garcia-Diaz, D. Damidot, O. Devès, B. Ruot, Influence of the intrinsic characteristics of mortars on biofouling by Klebsormidium flaccidum, Int. Biodeterior. Biodegradation. 70 (2012) 31–39. doi:10.1016/J.IBIOD.2011.10.017.

[25] M. D'Orazio, G. Cursio, L. Graziani, L. Aquilanti, A. Osimani, F. Clementi, C. Yéprémian, V. Lariccia, S. Amoroso, Effects of water absorption and surface roughness on the bioreceptivity of ETICS compared to clay bricks, Build. Environ. 77 (2014) 20–28. doi:10.1016/j.buildenv.2014.03.018.

[26] L. Graziani, E. Quagliarini, M. D'Orazio, The role of roughness and porosity on the self-cleaning and anti-biofouling efficiency of TiO2-Cu and TiO2-Ag nanocoatings applied on fired bricks, Constr. Build. Mater. 129 (2016) 116–124. doi:10.1016/j.conbuildmat.2016.10.111.

[27] L. Graziani, E. Quagliarini, A. Osimani, L. Aquilanti, F. Clementi, M. D'Orazio, The influence of clay brick substratum on the inhibitory efficiency of TiO2 nanocoating against biofouling, Build. Environ. 82 (2014) 128–134. doi:10.1016/j.buildenv.2014.08.013.

[28] A.Z. Miller, P. Sanmartín, L. Pereira-Pardo, A. Dionísio, C. Saiz-Jimenez, M.F. Macedo, B. Prieto, Bioreceptivity of building stones: A review, Sci. Total Environ. 426 (2012) 1–12. doi:10.1016/j.scitotenv.2012.03.026.

[29] P. Tiano, P. Accolla, L. Tomaselli, Phototrophic biodeteriogens on lithoid surfaces: An ecological study, Microb. Ecol. 29 (1995) 299–309. doi:10.1007/BF00164892.

[30] A.Z. Miller, A. Dionísio, L. Laiz, M.F. Macedo, C. Saiz-Jimenez, The influence of inherent properties of building limestones on their bioreceptivity to phototrophic microorganisms, 2009. https://link.springer.com/content/pdf/10.1007%2FBF03179212.pdf (accessed December 3, 2018).

[31] A.Z. Miller, M.A. Rogerio-Candelera, L. Laiz, J. Wierzchos, C. Ascaso, M.A. Sequeira Braga, M.

Hernández-Mariné, A. Maurício, A. Dionísio, M.F. Macedo, C. Saiz-Jimenez, Laboratory-induced endolithic growth in calcarenites: Biodeteriorating potential assessment, Microb. Ecol. 60 (2010) 55–68. doi:10.1007/s00248-010-9666-x.

[32] A.Z. Miller, N. Leal, L. Laiz, M.A. Rogerio-Candelera, R.J.C. Silva, A. Dionísio, M.F. Macedo, C. Saiz-Jimenez, Primary bioreceptivity of limestones used in southern European monuments, Geol. Soc. Spec. Publ. 331 (2010) 79–92. doi:10.1144/SP331.6.

[33] T.H. Tran, A. Govin, R. Guyonnet, P. Grosseau, C. Lors, D. Damidot, O. Devès, B. Ruot, Avrami's law based kinetic modeling of colonization of mortar surface by alga Klebsormidium flaccidum, Int. Biodeterior. Biodegrad. 79 (2013) 73–80. doi:10.1016/j.ibiod.2012.12.012.

[34] L. Graziani, E. Quagliarini, On the Modelling of Algal Biofouling Growth on Nano-TiO2 Coated and Uncoated Limestones and Sandstones, Coatings. 8 (2018) 54. doi:10.3390/coatings8020054.

[35] L. Graziani, E. Quagliarini, M. D'Orazio, TiO2-treated different fired brick surfaces for biofouling prevention: Experimental and modelling results, Ceram. Int. 42 (2016) 4002–4010. doi:10.1016/j.ceramint.2015.11.069.

[36] International Energy Agency, Guidelines and Practice, Annex XIV Condens. Energy. (1990). http://www.ecbcs.org/docs/annex_14_guidelines_and_practice.pdf.

[37] N.J. Rowan, C.M. Johnstone, R.C. McLean, J.G. Anderson, J.A. Clarke, Prediction of toxigenic fungal growth in buildings by using a novel modelling system, Appl. Environ. Microbiol. 65 (1999) 4814–4821.

[38] J.A. Clarke, C.M. Johnstone, N.J. Kelly, R.C. McLean, J.A. Anderson, N.J. Rowan, J.E. Smith, A technique for the prediction of the conditions leading to mould growth in buildings, Build. Environ. 34 (1999) 515–521. doi:10.1016/S0360-1323(98)00023-7.

[39] T. Ojanen, H. Viitanen, R. Peuhkuri, K. Lähdesmäki, J. Vinha, K. Salminen, Mold Growth Modeling of Building Structures Using Sensitivity Classes of Materials, Therm. Perform. Exter. Envel. Build. XI. (2010) 1–10. doi:10.1081/E-EEE2-120046011.

[40] K. Sedlbauer, Prediction of mould fungus formation on the surface of and inside building components,

2001. http://www.ibp.fraunhofer.de/content/dam/ibp/en/documents/ks_dissertation_etcm1021-30729.pdf.

[41] M. Krus, R. Kilian, K. Sedlbauer, Mould growth prediction by computational simulation on historic buildings, Museum Microclim. (2007) 185–189.

[42] 6-3-05/D WTA Merkblatt, Rechnerische Prognose des Schimmelpilzwachstumsrisikos, Fraunhofer IRB Versl. (2006).

[43] G. Arya, J. Singh, A mathematical model to predict Actinomycetes growth in building material, Int. J. Interdiscip. Res. Innov. 4 (2016) 88–96.

[44] S.P. Shukla, J. Kvíderová, J. Tříska, J. Elster, Chlorella mirabilis as a potential species for biomass production in low-temperature environment, Front. Microbiol. 4 (2013) 1–12. doi:10.3389/fmicb.2013.00097.

[45] S. Thelandersson, T. Isaksson, Mould resistance design (MRD) model for evaluation of risk for microbial growth under varying climate conditions, Build. Environ. 65 (2013) 18–25. doi:10.1016/J.BUILDENV.2013.03.016.

[46] J. Berger, H. Le Meur, D. Dutykh, D.M. Nguyen, A.C. Grillet, Analysis and improvement of the VTT mold growth model: Application to bamboo fiberboard, Build. Environ. 138 (2018) 262–274. doi:10.1016/j.buildenv.2018.03.031.

[47] ASTM D5589-09. Standard test method for determining the resistance of paint films and related coatings to algal defacement. American Society for Testing and Materials, (2009).

[48] L. Graziani, E. Quagliarini, A. Osimani, L. Aquilanti, F. Clementi, C. Yéprémian, V. Lariccia, S. Amoroso, M. D’Orazio, Evaluation of inhibitory effect of TiO2 nanocoatings against microalgal growth on clay brick façades under weak UV exposure conditions, Build. Environ. 64 (2013) 38–45. doi:10.1016/j.buildenv.2013.03.003.

[49] A. Viani, G. Cultrone, K. Sotiriadis, R. Ševčík, P. Šašek, The use of mineralogical indicators for the assessment of firing temperature in fired-clay bodies, Appl. Clay Sci. 163 (2018) 108–118. doi:10.1016/J.CLAY.2018.07.020.

[50] C. Coletti, G. Cultrone, L. Maritan, C. Mazzoli, Combined multi-analytical approach for study of pore system in bricks: How much porosity is there?, Mater. Charact. 121 (2016) 82–92. doi:10.1016/J.MATCHAR.2016.09.024.

[51] C. Coletti, G. Cultrone, L. Maritan, C. Mazzoli, How to face the new industrial challenge of compatible, sustainable brick production: Study of various types of commercially available bricks, Appl. Clay Sci. 124–125 (2016) 219–226. doi:10.1016/J.CLAY.2016.02.014.

[52] G. Cultrone, E. Sebastián, K. Elert, M.J. de la Torre, O. Cazalla, C. Rodriguez–Navarro, Influence of mineralogy and firing temperature on the porosity of bricks, J. Eur. Ceram. Soc. 24 (2004) 547–564. doi:10.1016/S0955-2219(03)00249-8.

[53] L. Graziani, E. Quagliarini, M. D'Orazio, Application of titania nanocoating to clay brick façades for biofouling prevention: efficiency and effect of substratum, Colloqui.AT.E. 1 (2014) 6.

[54] L. Graziani, E. Quagliarini, M. D'Orazio, Prevention of algal growth on clay façades by photocatalytic TiO2 nano- coating, (2015).

[55] L. Graziani, E. Quagliarini, F. Bondioli, M. D'Orazio, Durability of self-cleaning TiO2 coatings on fired clay brick façades: Effects of UV exposure and wet & dry cycles, Build. Environ. 71 (2014) 193–203. doi:10.1016/j.buildenv.2013.10.005.

[56] ASTM D4404-10. Standard test method for determination of pore volume and pore volume distribution of soil and rock by mercury intrusion porosimetry. American Society for Testing and Materials, (2010).

[57] UNI EN ISO 4287:2009. Geometrical Product Specifications (GPS) – Surface texture: Profile Method – Terms, Definitions and Surface Texture Parameters, International Standards Organization, (2009).

[58] T.H. Tran, N.D. Hoang, Estimation of algal colonization growth on mortar surface using a hybridization of machine learning and metaheuristic optimization, Sadhana - Acad. Proc. Eng. Sci. 42 (2017) 929–939. doi:10.1007/s12046-017-0652-6.

[59] J.H. Stock, M.W. Watson, Introduction to Econometrics, Third Edit, Pearson, 2015. http://library1.nida.ac.th/termpaper6/sd/2554/19755.pdf.

[60] W. Kong, S. Huang, F. Shi, J. Zhou, Y. Feng, Y. Xiao, Study on Microcystis aeruginosa growth in incubator experiments by combination of Logistic and Monod functions, Algal Res. 35 (2018) 602–612. doi:10.1016/J.ALGAL.2018.10.005.

[61] D.R. Tobergte, S. Curtis, Applied statistics using SSPS, Statistica, Matlab and R, Journal of Chemical Information and Modeling, 2013. doi:10.1017/CBO9781107415324.004.

Declaration of interests

☒ The authors declare that they have no known competing financial interests or personal relationships that could have appeared to influence the work reported in this paper.

☐The authors declare the following financial interests/personal relationships which may be considered as potential competing interests:

Authors Statement

Quagliarini: Supervision, Validation, Writing - Review & Editing.

Gregorini: Methodology, Formal Analysis, Writing – Original Draft.

D’Orazio: Supervision, Conceptualization.